Coastal Engineering 205 (2026) 104933

Contents lists available at ScienceDirect

Coastal Engineering

journal homepage: www.elsevier.com/locate/coastaleng

Influence of *Posidonia oceanica* accumulation on beach morphodynamics: A remote sensing study

S. Terracciano [a,*], J. Montes [b], R. Brunetta [a], P. Cabrita [a], P. Ciavola [a,c], C. Armaroli [d]

[a] Department of Physics and Earth Sciences, Università degli Studi di Ferrara, Via Saragat 1, 44122, Ferrara, Italy
[b] Earth Sciences Department, University of Cádiz INMAR, Avda. República Saharaui s/n, Puerto Real, 11510, Cádiz, Spain
[c] CNR-IAS Oristano, Institute for the Study of Anthropic Impact and Sustainability in the Marine Environment, Loc. Sa Mardini, 09710 Torregrande, Oristano, Italy
[d] Department of Biological, Geological and Environmental Sciences, Alma Mater Studiorum – University of Bologna, via Zamboni 67, 40126, Bologna, Italy

ARTICLE INFO

Keywords:
Satellite-derived shoreline
Posidonia banquette
Ecogeomorphology
Beach-dune interaction

ABSTRACT

Beach morphology is influenced by climate-related changes, such as rising sea levels, shifting weather patterns, and storms, as well as human activities, making continuous monitoring essential for understanding its evolution. Within this dynamic context, some beaches develop morphological features that help attenuate the impact of high-energy events, effectively acting as natural barriers against coastal erosion and flooding. This research explores the role of *Posidonia oceanica* banquettes, natural seagrass accumulations, in influencing beach dynamics, shoreline stability, and dune development, processes that are common along much of the Mediterranean coast. The study developed a new methodological approach by integrating aerial ortophotos with high-temporal-resolution multispectral satellite imagery, to analyse beach evolution in the presence of *Posidonia* banquettes, with a focus on the impact of storm events. This approach examines shoreline, dune, and Posidonia accumulations through a combination of remote sensing techniques, enabling both medium-term through Satellite-Derived Shoreline (SDS) (~10 years) and long-term analyses (~70 years) using orthophotos. The results highlight the complex interactions between human activities, storm events, and natural processes, particularly the role of *Posidonia* accumulation in shaping beach and dune morphology. Medium-term analysis has offered detailed perspective on recent beach changes, illustrating fluctuations in *Posidonia* berms related to storm events and correlating shoreline positions with dune evolution. Meanwhile, long-term orthophotos analysis has provided insights into sediment transport dynamics and revealed trend patterns over extended timeframes. This integration of SDS data and aerial imagery leveraged the identification of "hotspot areas" by analysing the relationship between shoreline changes and dune toe retreat.

1. Introduction

Over the past 100 years, climate-driven sea-level rise and shifting weather patterns have contributed to increasing beach erosion (Ranasinghe, 2016). In areas with well-developed dunes, these systems provide crucial natural protection against coastal erosion and storm events (Roig-Munar et al., 2019). However, in regions where dunes are small, sparsely vegetated, or have been altered by human development, beaches are more vulnerable to erosion, as the dunes no longer serve as an effective buffer (Fernández-Montblanc et al., 2020; Harley and Ciavola, 2013) processes. A notable example is the presence of the endemic seagrass *Posidonia oceanica (L.)*, which can help mitigate the impact of coastal storms on many Mediterranean beaches (Simeone and De Falco, 2013).

This seagrass, which colonizes the seafloor, has leaves that are washed ashore by wind and wave activity at the end of its life cycle. Once deposited on beaches, these leaves form natural barriers and accumulate on the beach in the form of banks known as *banquette* (Simeone et al., 2013). Its presence on beaches depends on various factors (e.g., beach morphology, wave dynamics and breaking type), and the accumulation of *Posidonia oceanica* leaves during low energy periods provides temporary and effective protection against erosion, particularly in areas where dunes or other natural barriers are degraded (De Falco et al., 2008). Recent studies have highlighted how *Posidonia oceanica* tends to accumulate after storm events during subsequent calm conditions (Gómez-Pujol et al., 2013). However, while the deposition

* Corresponding author.
E-mail address: sabrina.terracciano@unife.it (S. Terracciano).

https://doi.org/10.1016/j.coastaleng.2025.104933
Received 29 July 2025; Received in revised form 5 December 2025; Accepted 8 December 2025
Available online 17 December 2025

process is fairly well understood and widely agreed upon, the dynamics of its removal from the beach under wave action remain an open question. Some authors suggest that *Posidonia* is often quickly eroded under higher wave conditions, following an annual cycle (Simeone et al., 2013). Others argue that banquette erosion occurs mainly during calm sea conditions and only sporadically during storm events (Fernandez-Mora et al., 2025). The debate on the actual role of *Posidonia oceanica* in beach dynamics and its function in protecting against storm is still ongoing. Some authors argue that *Posidonia* debris aids sediment deposition, acting as a trap for sediment and reducing its potential to be transported during storm events (De Falco et al., 2008; Simeone and De Falco, 2013). Additionally, the presence of seagrass accumulations functions as a wave energy dissipator, limiting sediment losses away from the emerged beach (Sánchez-González et al., 2011). Laboratory studies have demonstrated that the size of the banquette plays a crucial role, as greater spatial dimensions, especially a wider distance between the foreshore and backshore, result in more effective attenuation compared to smaller ones (Astudillo-Gutierrez et al., 2024; Sierra et al., 2025). However, some researchers remain unconvinced of its actual protective role against storm events due to the limited permanence of the *banquette* on the beach. Gómez-Pujol et al. (2013) observed that *Posidonia oceanica* berms tend to remain on beaches for a relatively short period, often not long enough to serve as an effective protective element against storms, which can occur when the *Posidonia* has already disappeared from the beach. Nonetheless, the effectiveness of this protective mechanism can be compromised by human activities, such as the removal of seagrass deposits for aesthetic purposes or touristic exploitation of beaches, which disrupts these natural processes. Under beach management policies, seagrass banquettes are often considered as waste and a visual disturbance that can limit tourism (Simeone and De Falco, 2013), leading local authorities to carry out beach cleaning operations. In the best cases, this involves temporarily relocating the banquette to a designated area of the beach before the summer season and restoring it before winter, as in the case of Alghero in Sardinia (Manca et al., 2013). In the worst cases, it entails complete removal and disposal, either in designated facilities or behind the dune system (Simeone and De Falco, 2013). In all cases, it was observed that the relocation or removal of the banquette results in the loss of approximately 70 % of the trapped sediment (Astudillo et al., 2023). In this context, the monitoring of beaches where *Posidonia oceanica* accumulates is critical for understanding the dynamic interactions between seagrass deposits and the beach-dune system (Enríquez et al., 2019). To fully capture the complexity of coastal evolution, a multi-scale approach is essential, integrating global patterns with local processes (Hunt et al., 2023). Shoreline dynamics have been extensively studied using both aerial imagery and video monitoring. Aerial images provide valuable insights at regional and local scales over extended time periods (Quang et al., 2021), while video imagery offers high temporal and spatial resolution, although it is limited to the area framed by the camera and its fixed position (Arriaga et al., 2022). The emergence of new technologies, particularly satellite-derived shoreline (SDS) mapping, presents a promising opportunity to address these limitations, enabling the study of shoreline evolution from global to local scales with a higher temporal resolution (Cabezas-Rabadán et al., 2025). Therefore, one of the key challenges of this technology lies in the availability of algorithms capable of accurately extracting shoreline data from satellite imagery (Darwish, 2024; Vitousek et al., 2023; Zambrano-Medina et al., 2023).

In this regard, the development of algorithms for the semi-automatic extraction of shoreline positions has significantly improved medium and long-term analyses, as some of these can leverage free access to open data services (such as Copernicus or USGS), which provide a vast array of satellite images with high spatial, temporal and spectral resolution (Pardo-Pascual et al., 2012). These algorithms enable the use of multispectral satellite sensors to analyse image bands by applying extraction methods at both pixel and sub-pixel level. There are multiple algorithms for automatic shoreline extraction, ranging from pixel-level methods, which tend to produce larger errors, to more advanced techniques that improve shoreline accuracy by estimating its position within individual pixels. This is achieved by integrating information from neighbouring pixels to generate a smoother and more continuous shoreline contour. In particular, the CoastSat algorithm (Vos et al., 2019) utilizes the Marching Squares method, which, after classifying the image using the Modified Normalized Difference Water Index (MNDWI), helps to reduce the staircasing effect typically seen at the pixel level, generating a more refined land/water contour. SHOREX and SAET (Palomar-Vázquez et al., 2023; Pardo-Pascual et al., 2012), instead, rely on the Max Gradient method, which detects the shoreline by identifying the maximum variation in reflectance between land and water, improving accuracy at a sub-pixel level. Additionally, some algorithms use Soft Classification techniques, which assign probabilistic values to each pixel, estimating the percentage of land or water presence to further enhance shoreline delineation (Vos et al., 2023b).

Nevertheless, these algorithms are subject to errors, as the shoreline is automatically extracted from satellite images with mid-resolution, such as 10–20 m for Sentinel-2 and 15–30 m for Landsat 8 and Landsat 9. Additionally, SDS algorithms are frequently applied on beaches with diverse spectral reflectance characteristics, such as variations in sand colour and the slope of submerged and emerged beach, which can influence the accuracy of shoreline extraction (Cabezas-Rabadán et al., 2025). Shoreline detection is particularly challenging on beaches where *Posidonia oceanica* is present. Seagrass banquettes can significantly alter the spectral properties of the scene, complicating the distinction between sand, vegetation, and water. This complexity is further increased by the maturity stage of the banquette, which can range from wet to moist or dry, with sand content varying according to its position on the beach (backshore or foreshore)(Simeone, 2008). This often leads to inaccuracies in traditional shoreline extraction methods, underscoring the need for SDS techniques specifically tailored to seagrass-rich environments. Therefore, to assess the error associated with shoreline extraction in these contexts, a validation analysis is necessary. This should be conducted using field data acquired simultaneously with the satellite passage, both in the presence and absence of *Posidonia oceanica*.

Traditional studies on the deposition-erosion cycle of *Posidonia oceanica* involve the use of video monitoring techniques (Trogu et al., 2023) or field data (Corbí et al., 2018). One key advantage of video monitoring techniques is their ability to capture hour-by-hour fluctuations of the seagrass banquette on a specific beach, while also enabling the classification of banquette accumulations thanks to the large volume of images and high spatial resolution (Sabato et al., 2023).

Therefore, the aim of this study is to develop a new methodological approach to understand beach dynamics in the presence of *Posidonia oceanica* banquettes, using aerial photographs and satellite imagery for analysing medium- and long-term evolution. The study is structured to examine beach evolution not solely from the perspective of shoreline changes but by considering dunes and banquettes presence or absence.

2. Material and methods

2.1. Study area

The Gulf of Oristano is a semi-enclosed basin located on the western coast of Sardinia (Italy), covering an area of approximately 150 km^2, with an average depth of 15 m and a maximum depth of 25 m (Fig. 1A). Its coastline consists of long sandy beaches, intermittently divided by human-made structures including the Industrial Port of Oristano, while the hinterland is characterized by extensive salt marsh systems, cultivated fields and several coastal lagoons. This stretch features beaches of varying widths, transitioning from broader, urbanized shores in the north to narrower, more natural ones in the south. Next to the industrial port there is the mouth of the Tirso River—the largest river in Sardinia—dammed since the early 20th century (Simeone et al., 2024). Weather and sea conditions are influenced by two predominant wind

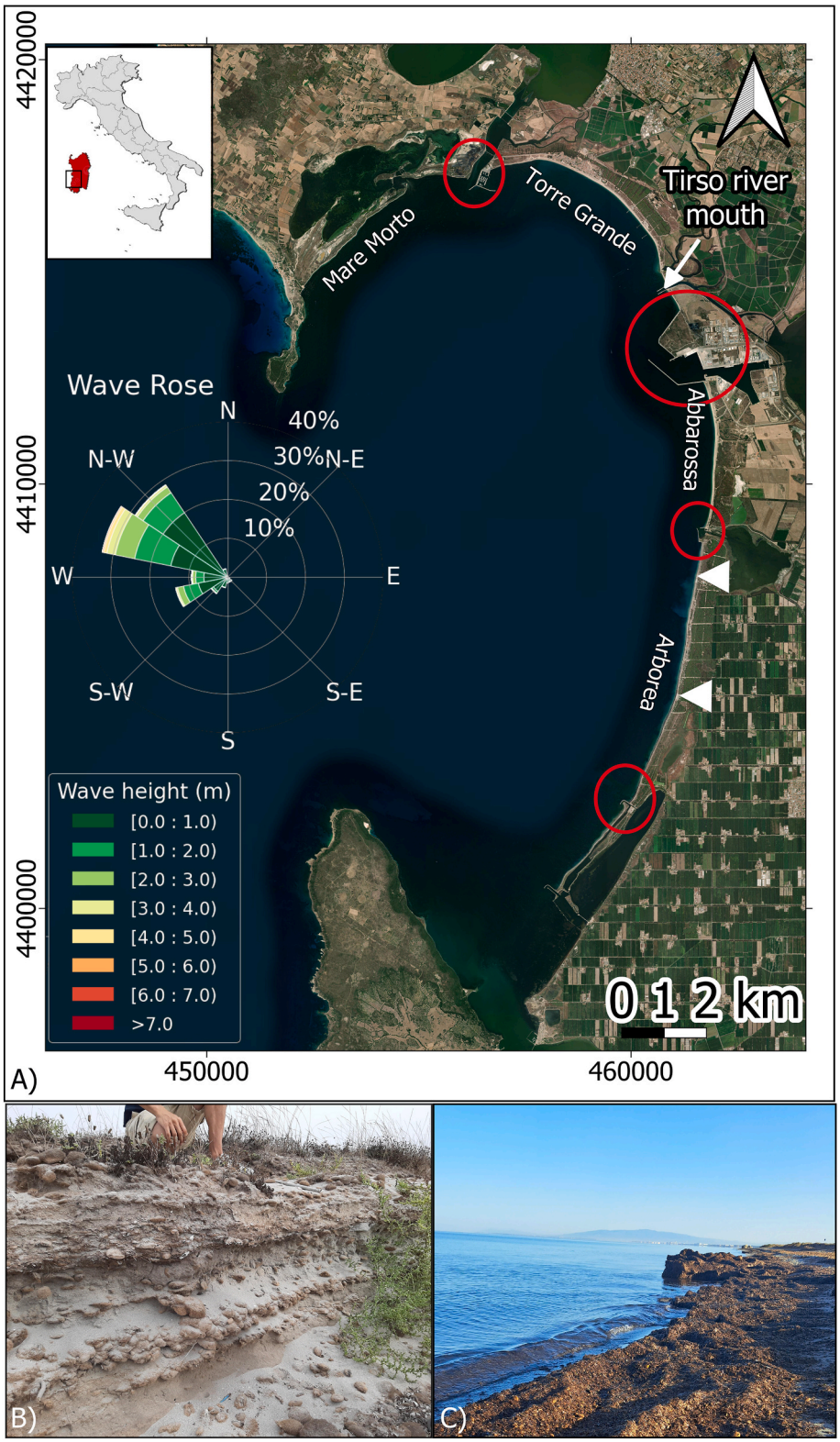

Fig. 1. A) Study area of the Gulf of Oristano, red circles indicate the position of the jetties and the industrial port of Oristano and the white triangle the turistic structures as beach resort and club. Basemap google satellite; B) Dune toe on Arborea beach where layering of sand and Neptune balls is visible; C) Banquettes of *Posidonia oceanica* on Arborea beach.

regimes: the northwest wind, known locally as mistral, which is the most powerful, and winds from the southwest (*Libeccio*). The maximum tidal range at Spring Tides is 20 cm (Cucco et al., 2006). Arborea beach (Fig. 1A), situated in the southern part of the Gulf of Oristano, faces the northwest and is primarily exposed to storm events driven by the Mistral north-westerly winds. The beach is characterised by the presence of *Posidonia oceanica* banquettes (Fig. 1C), which naturally accumulate on the foreshore and are generally deposited in large quantities in the southern and northern parts of the bay near the jetties of the ports. Additionally, substantial quantities of Neptune balls, also known as

Egagropiles, are present, typically accumulating at the dune toe and gradually becoming embedded within the dune itself (Fig. 1B). Neptune balls result from the interaction of wind and sand with *Posidonia* deposits through the breaking-up of leaves into filaments.

The uniqueness of Arborea beach, within the context of the Gulf of Oristano, is also attributed to its low tourist pressure. Visitors are primarily concentrated in the central area, where a beach club is located, and in the northern area, where a beach resort was constructed between 2006 and 2010 (Fig. 1A). These zones are periodically cleaned from *Posidonia* detritus, which is then deposited in front of the dune. This practice is carried out "following screening aimed at separating sand from organic material, as well as the removal of intermixed waste of anthropogenic origin, also for the potential recovery of sand to be used for beach nourishment," as outlined in the Italian law *Legge Salvamare* (L. May 17, 2022, n° 60 - art. 5). Meanwhile, there are some areas that remain completely untouched or have received only infrequent interventions.

2.2. Workflow

Fig. 2 presents the workflow of the study, which consists of using aerial and satellite images as the primary sources. Shorelines were extracted from aerial photographs spanning from 1954 to 2022 through photointerpretation, providing a detailed record of long-term shoreline changes. On the other hand, shorelines were extracted from satellite images (Sentinel-2 and Landsat 9) to capture medium-term changes. The extraction of satellite-derived shorelines involved a validation process to ensure accuracy and to determine, in the presence or absence of banquettes, which physical proxy is represented by the satellite-derived shoreline (i.e., the instantaneous water line or the wet/dry line). This process compared shorelines acquired through fieldwork using GNSS RTK with those extracted using two different algorithms: CoastSat (Vos et al., 2019) and SAET (Palomar-Vázquez et al., 2023). Based on the validation results, the most accurate algorithm was selected for short-term analysis.

All spatial data, including aerial (obtained through photointerpretation) and SDS, were organized and managed in a geodatabase. The resulting dataset was then used to perform trend analyses using the DSAS tool (Himmelstoss et al., 2021). Additionally, the effect of shorelines on dune toe was examined by integrating data from satellite images and aerial photographs. This comprehensive approach allowed for an understanding of shoreline dynamics and the effects of environmental factors, such as the role of *Posidonia oceanica* banquettes on dune movement.

2.3. Banquette classification

Classifications of *Posidonia* banquettes are not always clearly defined or consistently addressed in the literature. Therefore, in Table 1 is proposed a classification based on field observations and a review of the available literature. It has been structured according to the level of activity of the banquette. For each category, a specific symbol has been created and an example image has been added to facilitate visualization.

2.4. Data collection

The collected data include aerial photographs, satellite imagery and GNSS measurements. First, aerial images were obtained through the Web Map Service (WMS) provided by the Sardinia regional authority (Regione Autonoma della Sardegna, 2025). This service includes aerial photographs from various years, obtained in 1954 (panchromatic), 1968, 1977, 1997, 1999, 2003, 2006, 2010, 2013, 2016, 2019, and 2022 (Table 2). The positional uncertainty associated with each shoreline delineation (Table 2) was calculated following the approach proposed by Del Río and Gracia (2013), which combines three main sources of error: image resolution (R), georeferencing accuracy (G), and proxy interpretation error (D). The total uncertainty (E) was computed using the root-sum-square method. Since the shoreline proxy adopted in this

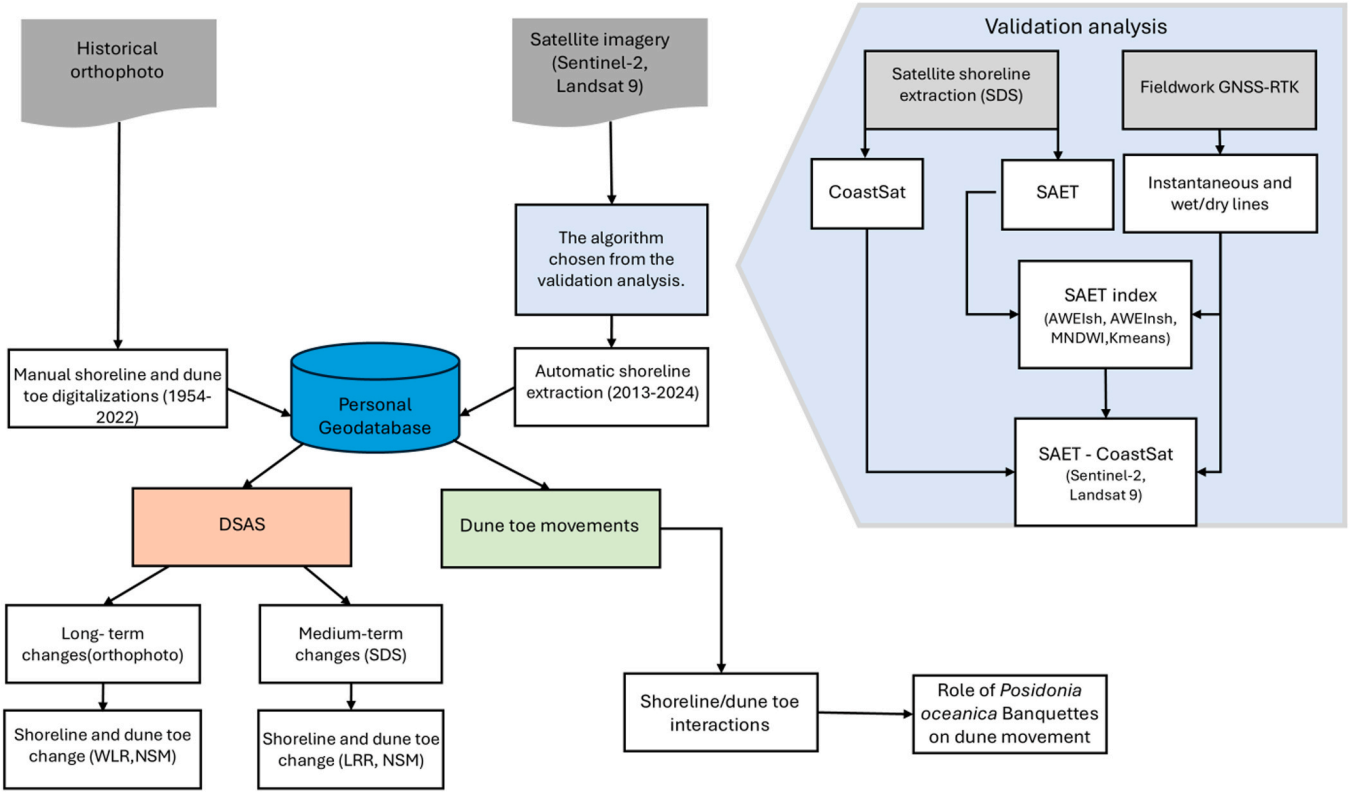

Fig. 2. – Workflow combining the use of historical orthophotos and satellite images.

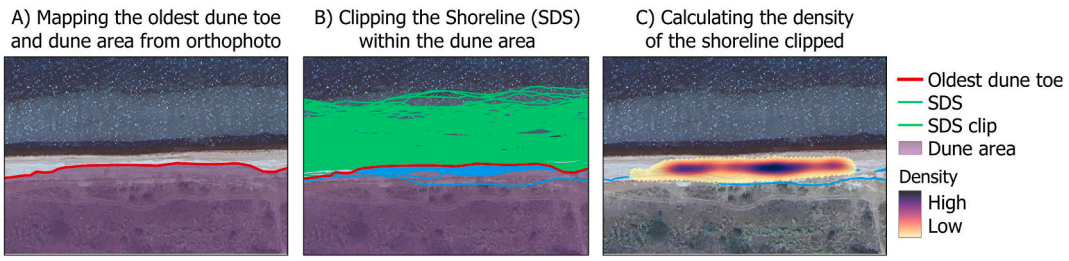

Fig. 3. – The image shows the workflow of the methodology for calculating density, divided into three phases, Basemap google satellite: A) digitization of the oldest dune toe and creation of a polygon representing the dune area; B) clipping of the SDS that fall within the dune area; C) calculation of the density of the clipped lines.

Table 1
– Classification of the different condition states of *Posidonia oceanica* banquettes observed by the authors in the field. Each banquette condition is accompanied by a representative symbol and an example image. The image corresponding to the "Stable" condition was taken from Google Maps, image credits: Stefano Orrú (2020).

Banquette Condition	Description	Symbol	Example image
Active	Freshly deposited banquettes represent ephemeral accumulations of *Posidonia oceanica* debris, the landward limit is the maximum run-up. These formations exhibit variable dimensions and are characterized by a limited sedimentary content in the foreshore zone and a higher sediment content in the backshore zone (Simeone, 2008; Simeone and De Falco, 2012, 2013; Astudillo-Gutierrez et al., 2025). They display a high water content, often forming shallow, pond-like depressions. Structurally, freshly deposited banquettes are highly mobile and unconsolidated, with occasional extensions into the swash zone where floating necromass may be observed. They are typically dark brown in color, reflecting the high water content and the recent state of plant death.		
Semi-active	Intermediate-aged, dried banquettes represent accumulations of *Posidonia oceanica* debris that have been deposited for a moderate period (i.e., from a few days to weeks) and have undergone partial desiccation and erosion. Located near the landward limit of the beach, corresponding to the maximum run-up zone, these formations exhibit variable dimensions and are characterized by a significant sedimentary content (Simeone, 2008), as they are part of the backshore section of the banquette that has not yet been eroded. The water content is low, and structurally, they form a compact mass, partially covered by sediment. The overall color appears lighter, resembling that of the surrounding sediment.		
Stable	Long-term persistent banquettes are accumulations of *Posidonia oceanica* debris that remain in place for extended periods (i.e. from months to years) and show signs of initial vegetation colonization (Del Vecchio et al., 2013). These formations typically extend over 10 m in length and are characterized by a high sediment content, while their water content is largely influenced by atmospheric conditions. A key feature of these banquettes is the presence of vegetation, with the compact structure resulting from root growth and sediment entrapment.		
Additional category	**Description**	**Symbol**	**Example image**
Dispersed debris	Highly eroded banquettes are remnants of *Posidonia oceanica* accumulations that have undergone significant degradation, or result from the fresh deposition of small amounts of detached leaves. They are typically found as scattered, patchy deposits emerging from the surrounding sediment. These formations are characterized by a high sediment content and a variable water content, which depends on their position relative to the maximum run-up zone. Their dimensions are generally limited, ranging from a few centimeters up to a maximum of 1–2 m.		

study is the wet/dry line, the visible boundary between saturated and dry sand, the associated positional uncertainty (D) was estimated at 1.0 m, following standard values reported in the literature for this type of proxy (Moore, 2000; Ruggiero and Kaminsky, 2003). This choice is justified by the typically low tidal range in the Mediterranean and the moderate beach slopes observed in this area. In particular, the beach at Arborea is characterized by an average slope of approximately 5 %, as documented by (Cabrita et al., 2024), which supports a conservative yet realistic estimate of proxy uncertainty. Georeferencing errors (G) are estimated based on acquisition year and typical planimetric accuracies in similar photogrammetric contexts. Image resolution (R) values were obtained directly from metadata and reflect the spatial resolution of each orthophoto, ranging from 0.2 m in the most recent datasets to 1.0 m in older ones.

The satellite-derived shorelines were extracted from Landsat 8 images for the period from July 2013 to July 2015 and from Sentinel-2 images for the period from August 2015 to September 2024. A cloud cover threshold of 20 % was established for both satellite images to minimize the potential sources of data errors or misinterpretation.

GNSS RTK field surveys were performed on i) May 26, 2023, ii) October 10, 2023, iii) 15/022 024, and iv) April 07, 2024. The data collection consisted of the acquisition of the instantaneous water line (defined as the boundary between water and sand/banquette) and the wet/dry line (defined as the boundary between banquette and sand, when banquettes are present). Shorelines for validation were surveyed simultaneously with Sentinel-2 and Landsat 9 satellite overpasses (Landsat 9 has the same characteristics as Landsat 8, wich was used to obtain satellite-derived shorelines for the period July 2013–July 2015). Field data were acquired using a Trimble R8 RTK-GPS, with a nominal horizontal accuracy of 8 mm and a nominal vertical accuracy of 15 mm. The GPS was positioned along the shoreline, collecting data at a frequency of 1 Hz (1-s interval) through continuous acquisition.

Storm events were related to the shoreline analysis from satellite imagery through the analysis of the time series of significant wave

Table 2
– Summary of aerial images sources and the calculated uncertainty.

Year	Orthorectified	Spatial Resolution (m)	Data Source	Metadata Link	Georeferencing Error (G, m)	Proxy Error (D, m)	Total Uncertainty (E, m)
1954	Yes	1.0	Regione Autonoma della Sardegna	https://webgis2.regione.sardegna.it/geonetwork/srv/api/records/R_SARDEG:OWSCQ/formatters/xsl-view?output=pdf&language=ita&approved=true	2.0	1.0	2.4
1968	Yes	1.0	Regione Autonoma della Sardegna	https://webgis2.regione.sardegna.it/geonetwork/srv/api/records/R_SARDEG:22e55714-3d1f-49b6-847f-a926899c8056/formatters/xsl-view?output=pdf&language=ita&approved=true	2.0	1.0	2.4
1977	Yes	1.0	Regione Autonoma della Sardegna	https://webgis2.regione.sardegna.it/geonetwork/srv/api/records/R_SARDEG:AYCEY/formatters/xsl-view?output=pdf&language=ita&approved=true	2.0	1.0	2.4
1997	Yes	1.0	Regione Autonoma della Sardegna	https://webgis2.regione.sardegna.it/geonetwork/srv/api/records/R_SARDEG:8514adfb-02f8-4b84-8cd5-1d9d22b2ee65/formatters/xsl-view?output=pdf&language=ita&approved=true	1.5	1.0	2.0
2000	Yes	1.0	Regione Autonoma della Sardegna	https://webgis2.regione.sardegna.it/geonetwork/srv/api/records/R_SARDEG:RNVCI/formatters/xsl-view?output=pdf&language=ita&approved=true	1.5	1.0	2.0
2003	Yes	0.5	Regione Autonoma della Sardegna	https://webgis2.regione.sardegna.it/geonetwork/srv/api/records/R_SARDEG:XXLZR/formatters/xsl-view?output=pdf&language=ita&approved=true	1.0	1.0	1.5
2006	Yes	0.5	Regione Autonoma della Sardegna	https://webgis2.regione.sardegna.it/geonetwork/srv/api/records/R_SARDEG:MFOMJ/formatters/xsl-view?output=pdf&language=ita&approved=true	1.0	1.0	1.5
2010	Yes	0.5	Regione Autonoma della Sardegna	https://webgis2.regione.sardegna.it/geonetwork/srv/api/records/R_SARDEG:79aac9b0-46b6-407b-a92a-3c3cb94a8c89/formatters/xsl-view?output=pdf&language=ita&approved=true	1.0	1.0	1.5
2013	Yes	0.5	Regione Autonoma della Sardegna	https://webgis2.regione.sardegna.it/geonetwork/srv/api/records/R_SARDEG:6b5bd1ad-7730-4b2f-af64-59a7c69b14d1/formatters/xsl-view?output=pdf&language=ita&approved=true	1.0	1.0	1.5
2016	Yes	0.2	Regione Autonoma della Sardegna	https://webgis2.regione.sardegna.it/geonetwork/srv/api/records/R_SARDEG:54fa199b-7860-473d-9f06-a8256d3d5b79/formatters/xsl-view?output=pdf&language=ita&approved=true	0.5	1.0	1.2
2019	Yes	0.2	Regione Autonoma della Sardegna	https://webgis2.regione.sardegna.it/geonetwork/srv/api/records/R_SARDEG:c82b8535-50b8-4f00-8a5e-a3ae24c33030/formatters/xsl-view?output=pdf&language=ita&approved=true	0.5	1.0	1.2
2022	Yes	0.2	Regione Autonoma della Sardegna	https://webgis2.regione.sardegna.it/geonetwork/srv/api/records/R_SARDEG:b4355702-ed36-4f2e-97c8-07e65e785efc/formatters/xsl-view?output=pdf&language=ita&approved=true	0.5	1.0	1.2

heights (Hs) extracted from two products of the Copernicus Marine Environment Monitoring Service (CMEMS, https://marine.copernicus.eu). For the historical period, the reanalysis product GLOBAL_MULTIYEAR_WAV_001_032 (WAVERYS) was used. This global dataset provides 3-hourly Hs estimates based on the MFWAM model on a 0.2° regular grid (~20 km spatial resolution), covering the period from January 1980 to May 2023. For the most recent period, from the end of the reanalysis dataset to the end of 2024, the Mediterranean wave forecast system MEDSEA_ANALYSISFORECAST_WAV_006_017 was employed. This regional product is based on the WAM Cycle 6 model and provides hourly forecasts and analysis fields at a spatial resolution of approximately 4.6 km (1/24°), with coverage extending up to 10 days into the future and analysis fields available for the previous two years.

Significant wave height time series were extracted at the nearest grid cell corresponding to the study area coordinates (39.84 N, 8.39 E (EPSG:4 326)). Storm events were identified using a threshold corresponding to the 95th percentile of the Hs distribution over the entire combined dataset (reanalysis + forecast), along with a minimum storm duration of 12 h and a meteorological independence criterion of 6 h to distinguish separate events (Harley, 2017).

2.5. SDS extraction and validation

Shoreline features were extracted using two different algorithms for multispectral images: Coastsat (Vos et al., 2019) and SAET (Palomar-Vázquez et al., 2023). The accuracy of the extraction was evaluated by comparison with *in situ* data measured with the GNSS RTK, used as ground truth. The distances between SDS shorelines and the in-situ shoreline were calculated and the RMSE values along with the standard deviation were computed. The technique was first employed to select the index of the SAET algorithm that best approximates the real case and exhibits the smallest error. Indeed, the SAET algorithm provides the option to choose from three different indices—Modified Normalized Difference Water Index (MNDWI), Automated Water Extraction Index for shadow (AWEIsh), and Automated Water Extraction Index for non-shadow (AWEInsh)—as well as one classification method (K-means). CoastSat, on the other hand, exclusively utilizes the MNDWI index, that excludes the preliminary error analysis required by SAET.

Once the algorithm and its index with the lowest error were selected, they were used to conduct the medium-term analysis using the available satellite images (Landsat 8, with the same characteristics as Landsat 9, from 2013 to 2015, and Sentinel-2 from 2015 to 2024.). The extracted shorelines were visually inspected to ensure that they accurately

followed the actual coastline. Lines that deviated critically, such as those extending far offshore or inland, or those forming unrealistic loops and self-intersections, were identified as artifacts of the extraction process and discarded. After this filtering step a total of 389 shorelines used in the analysis. Additionally, to analyse shoreline displacement, distances were measured along equally spaced cross-shore transects, using as a reference the average shoreline position from the first year (Briceño de Urbaneja et al., 2024).

2.6. Processing of aerial images

To understand the dynamics of longshore transport and the evolution of the beach, a long-term analysis was conducted using the shorelines photo-interpreted on aerial photos. Two different proxies were used for the analysis: the dune toe and the shoreline. The dune toe was defined based on the seaward limit of dune vegetation, while the shoreline was identified using the wet/dry line, following the criteria of (Boak and Turner, 2005). Both features were digitized at a scale of 1:500. In areas where *Posidonia oceanica* seagrass accumulations were present, the boundary between the banks and the sand was used as the reference instead (Martín Prieto et al., 2018).

2.7. Trend analysis

The Digital Shoreline Analysis System (DSAS) tool (V 5.0) was employed to analyse trends (Himmelstoss et al., 2021). This tool utilizes multiple statistical methods to establish the relationship between the shorelines and requires certain parameters to be set by the operator. Initially, an offshore baseline was edited parallel to the shorelines. Subsequently, transects perpendicular to the baseline spaced 20 m were generated. Finally, various statistical analyses were applied to the points where the transects intersect the shorelines, following the methodology outlined by Himmelstoss et al. (2018): the Linear Regression Rate (LRR) and Weighted Linear Regression (WLR), which represent the rates of change in meters per year, and the Net Shoreline Movement (NSM), which represents the distance between the oldest and the most recent shoreline. The first are determined by the slope of the regression line, which is calculated based on the intersection points of time and distance from the baseline. The tool was employed to perform both medium-term analyses (using satellite images) and long-term analyses (using orthophotos) of the shoreline and dune toe.

2.8. Shoreline-dune toe interaction

An analysis was conducted to assess the interaction between shoreline movements and the dune toe, especially after storm events. An innovative method was applied to establish the connection between shoreline position and dune movement by identifying "hotspot areas" where the dune is more vulnerable and the shoreline may reach the dune toe. In order to establish a threshold using the only orthophotos available for the considered time series (the period considered for this analysis is 2016–2022, due to the availability of orthophotos and satellite imagery), two dune toe lines were used as thresholds: the first included shorelines that overpass the 2016 dune toe between 2016 and 2018; the second included shorelines from 2019 to 2022 that overpass the 2019 dune toe. Using these lines, a density map was then created with the Kernel Density tool in ArcMap, following the approach of Rizzo et al. (2022). The Kernel Density tool calculates the magnitude per unit area from line features (in this case, shorelines overpassing the dune toe) using a kernel function. Specifically, it applies a Gaussian function that spreads the influence of each input line across a specified search radius. In this study, the radius was set to 20 m, corresponding to twice the maximum distance calculated between the filtered shorelines), which produces a smooth and continuous surface. The output raster reflects the density of lines within that radius, with higher values where multiple features (e.g., shoreline exceedances) cluster spatially (Fig. 3). This allows for the identification of the highest frequency of shoreline contact with the dune toe over time. Subsequently, only shorelines corresponding to storm events occurring within a 9-day temporal window were selected. Storm events were identified using the same Peak Over Threshold (POT) parameters described in Section 2.4, specifically the 95th percentile of Hs as a threshold, a minimum storm duration of 12 h, and a 6 h meteorological independence criterion. This interval was determined by calculating the satellite revisit time for the study area based on the total number of available useful images. The characteristics of individual storm events occurring within this timeframe were then related to shoreline overpassing of the dune toe. Additionally, the presence or absence of *Posidonia oceanica* before and after each event was assessed through visual inspection of the satellite imagery used in the study. A symbol from Table 1 was assigned to each case based on the observed type of banquette, if present. In case of absence of banquette, a symbol corresponding to the "dispersed debris" category was assigned if observed; otherwise, no symbol was used. The images used for this assessment corresponded to the first available date after the storm event and the first available date before it. If cloud cover prevented clear observation, a "no data" value was assigned when no suitable imagery was available within the 9-day window.

3. Results

3.1. Long-term analysis (1954–2022)

The long-term analysis of Arborea beach (Fig. 4) reveals that the area is experiencing variable trends without a uniform long-term direction. The beach was divided into four zones based on exposure and preliminary observations. Area 1 is located in the southern part, Areas 2 and 3 in the central part, and Area 4 in the northern part.

High erosional trends are observed in the southernmost portion of Arborea Beach (Area 1, Fig. 4A), with a WLR ranging from approximately −0.10 to −0.40 m/y. Moving slightly northward within the same area, more stable conditions appear, with WLR values between −0.10 and 0.10 m/y. Looking at the temporal evolution (Fig. 4B), an initial accretion phase is evident until around 1968, followed by a more stable phase during the 1980s. This stability is then followed by another accretion phase that continues until the early 2000s, when a clear erosional trend begins. This trend reaches a maximum retreat of nearly −10 m around 2013, before returning to a more stable condition by 2022. The linear regression indicates $R^2 = 0.34$ and $p = 0.045$. Fig. 4C highlights the predominance of erosion in this area, with accretional values occurring only in the northernmost part of Area 1.

A stable or accretionary zone, with WLR values ranging from 0.10 to 0.40 m/y, is observed in Area 2, followed by an erosional trend where the WLR decreases to about −0.10 to −0.40 m/y. Observing the average trends of the area during the study period (Fig. 4B), accretion peaks around the 2000s, after which erosion becomes dominant and remains constant until the end of the analysis, reaching a retreat of approximately 10 m inland. In this case, the regression shows $R^2 = 0.21$ and $p = 0.135$, indicating the absence of a statistically significant trend. In Fig. 4C, maximum erosion rates of −0.3 m/y are observed, but overall, the area shows lower average values compared to Area 1, generally ranging between −0.1 and −0.2 m/y.

In Area 3 (Fig. 4A), erosion rates ranging from −0.10 to −0.40 m/y are visible across the entire area, with small stable zones located in the southern and northern portions. In this part of the beach, a trend similar to that of Area 1 is observed, especially in the early years, although conditions appear more stable during the 2000s (Fig. 4B). Furthermore, erosion is less severe, reaching a maximum inland retreat of about 5 m, with a total shoreline shift of approximately 7 m inland by 2022 compared to 1954. The regression yields $R^2 = 0.42$ and $p = 0.022$. Additionally, Fig. 4C shows that erosion rates in this area are generally lower than those observed in Areas 1 and 2.

Only the northernmost section of the beach (Area 4, Fig. 4A) shows

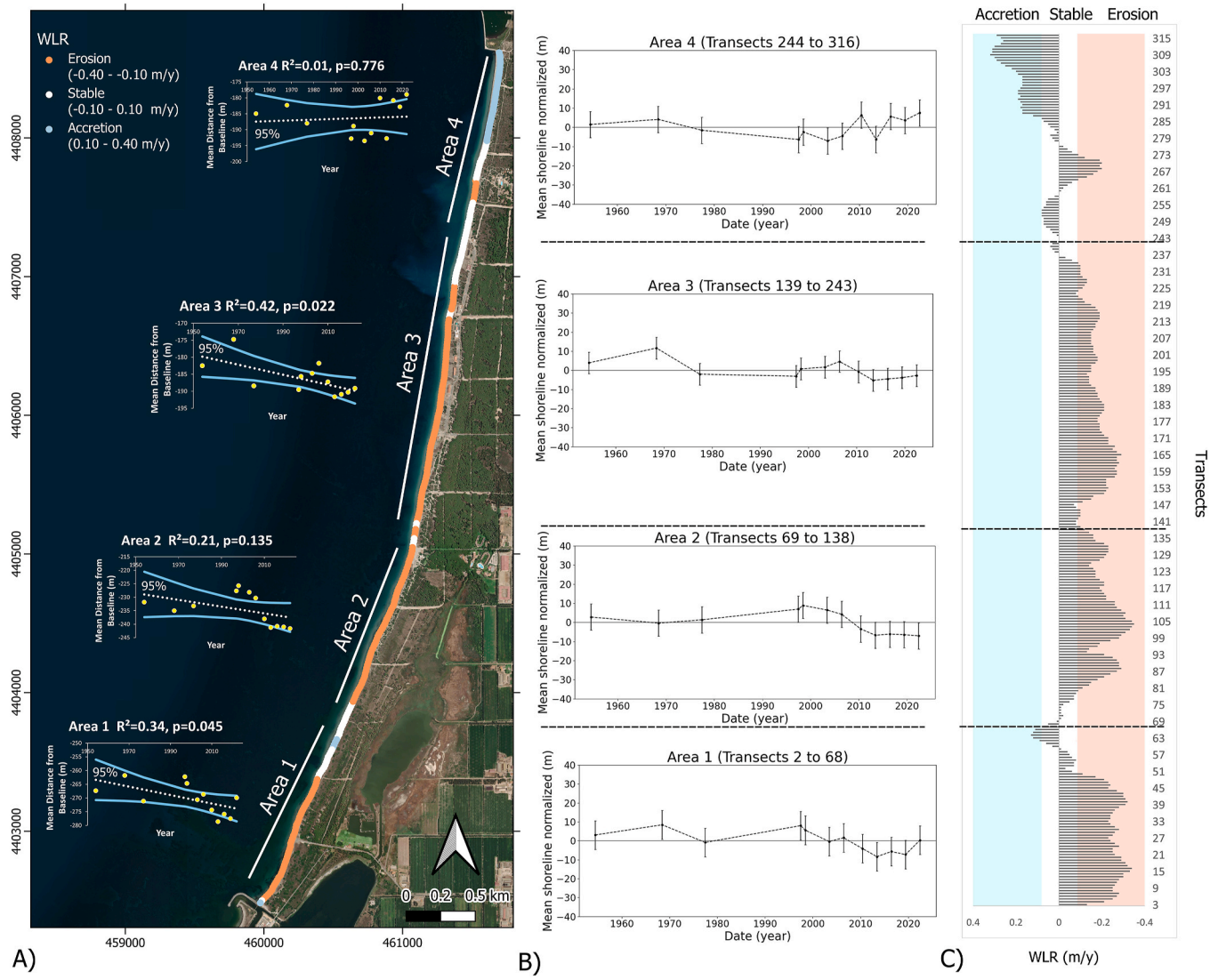

Fig. 4. – Long term analysis (1954–2022). Basemap google satellite; A) Map of Weighted Linear Regression (WLR). For each area, the inset graphs display the linear regression line, 95 % confidence interval, R^2, and p-value of the trend; B) Temporal Shoreline Position Anomaly, Normalized to the Historical Mean (1954–2022); C) Graphical visualization of WLR.

an accretion zone with a rate of about 0.2 m/y, featuring more stable areas in the southern part and a small erosional zone near the tourist residence. The trend observed in this area (Fig. 4B) is opposite to that of Area 1, with relatively constant erosion between 1999 and 2006, followed by an accretion peak in 2010 and a subsequent erosion peak in 2013. After that, an accretion trend continues until 2022. Additionally, between 2013 and 2022, an accretion of approximately 20 m is observed. The regression for this area shows $R^2 = 0.01$ and $p = 0.776$, indicating no significant long-term trend. Finally, Fig. 4C highlights the predominance of the accretional regime, with stable areas and a localized erosional zone where rates reach up to −0.2 m/y.

3.2. SDS accuracy assessment

The error analysis carried out to identify the most accurate SAET index indicated that AWEInsh was the most effective in delineating the water–land boundary, consistently yielding the lowest error values across many case studies and banquette conditions, with RMSE ranging from 2.32 m to 3.98 m. This performance was consistent in both areas with and without *Posidonia* presence (Fig. 5) and is further illustrated in the Appendix (Figure A 1 Figure A 2 and Table A.1), where plots with the differences between the surveyed shoreline and SDSs, Q–Q plots, and bias values are provided to support the interpretation of residuals' distribution and shoreline displacement.Accordingly, it was selected as the preferred index. Moreover, the figure shows that the AWEIsh index yields relatively low error values in conditions of active and semi-active banquette, while it displays the highest error values among all indices when *Posidonia* is in condition of disperses debris or absent. This limits its applicability in real-world scenarios, where *Posidonia oceanica* presence can vary significantly. The MNDWI (the same index used by CoastSat), on the other hand, shows error values comparable to those of the selected AWEInsh, except on the last date, when the absence of *Posidonia oceanica* corresponds to a significantly higher error.

The error analysis revealed that the CoastSat algorithm, when applied with its default settings using the MNDWI index, resulted in an RMSE greater than 10 m (Table 3). In contrast, the SAET algorithm and index combinations achieved lower errors, with the AWEInsh index showing the best performance among the tested alternatives. Accordingly, CoastSat and the other SAET combinations were excluded from the medium-term analysis, and SAET with the AWEInsh index was selected as the preferred method for shoreline extraction.

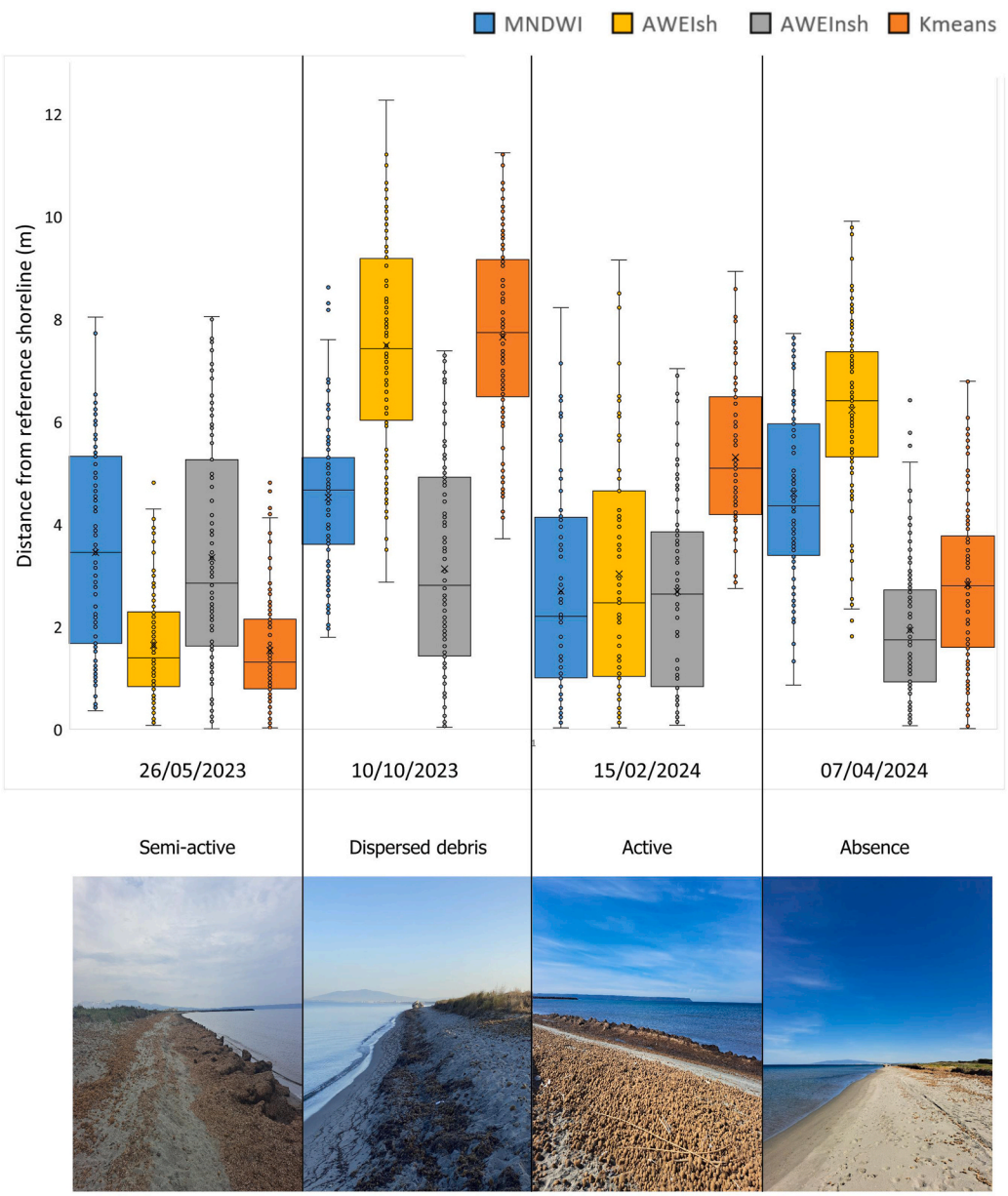

Fig. 5. Shoreline detection accuracy across four different *Posidonia* banquette conditions using MNDWI (blue), AWEIsh (yellow), AWEInsh (grey), and K-means (orange). Boxplots represent the distance (in meters) from the detected shoreline to a reference shoreline acquired in the field using GNSS-RTK measurements. Each point corresponds to a single transect; boxes indicate the interquartile range (25th–75th percentile), the horizontal line within each box represents the median, whiskers extend to 1.5 times the interquartile range, and points outside the whiskers denote outliers. The four panels correspond to distinct field conditions: semi-active *banquette* (May 26, 2023), dispersed debris (October 10, 2023), active banquette (February 15, 2024), and complete absence banquette (April 07, 2024), as shown in the photos below.

3.3. Medium-term analysis (2013–2024)

In the medium-term analysis the Linear Regression Rate (LRR) was selected as the statistical method (Fig. 6A–C). The analysis of the two figures reveals that, in Area 1, erosion rates are most pronounced in the extreme southern sector, reaching values close to −2.8 m per year. The central sector (Areas 2 and 3) shows both erosional and accretional zones, but with lower magnitudes compared to Area 1, reaching a maximum erosion rate of −1 m/y and a peak accretion rate of 0.5 m/y. The northern sector (Area 4) exhibits shoreline accretion, with maximum rates approaching +2 m/y.

Fig. 6B further corroborates these findings, showing that the central and northern sectors, corresponding to Areas 3 and 4, respectively, are consistent with the patterns previously identified in the long-term analysis. Overall, across all four areas, it is difficult to identify a clear and consistent trend in this analysis, particularly in Area 1, which is characterized by a highly irregular pattern. The error bars also highlight the spatial variability of the data, as they represent the average standard deviation across transects for each area. In Area 1, the error bars are wider, whereas they are narrower in Area 3.

Despite the absence of an overall trend in Area 1, localized patterns of shoreline advance and retreat are evident. A notable example occurs at the beginning of 2023, when, following an accretion phase that begins in early 2022, with a seaward shift of nearly 25 m, a shoreline retreat of approximately 40 m is recorded. A similar pattern is also observed in Area 2, although with a smaller displacement of about 30 m. Subsequently, the shoreline position remains relatively stable through 2024. Another example can be observed in 2017, although it is less pronounced than the previously described case. Following an accretion phase of approximately 20 m, a shoreline retreat of about 25 m occurred,

Table 3
– Error analysis for SAET (selected index AWEInsh) and CoastSat for satellite Sentinel-2 and Landsat-9.

Algorithm	RMSE of the algorithm	Date	Error (m)	Sentinel-2 Instantaneous water line	Wet/Dry line	Landsat-9 Instantaneous water line	Wet/Dry line
CoastSat	<10 m	May 26, 2023	RMSE	16.79	22.99	23.41	26.95
			St.dev	6.93	8.35	4.07	3.95
		October 10, 2023	RMSE	12.55	15.41		
			St.dev	1.24	1.52		
		February 15, 2024	RMSE	13.46	21.74		
			St.dev	2.85	4.12		
		April 07, 2024	RMSE	11.68	13.46		
			St.dev	3.99	4.23		
		MEAN		13.62	18.40		
SAET	>3m	May 26, 2023	RMSE	3.98	6.00	2.55	6.14
			St.dev	1.97	2.48	2.33	2.51
		October 10, 2023	RMSE	3.73	1.95		
			St.dev	1.40	1.05		
		February 15, 2024	RMSE	3.19	5.76		
			St.dev	2.09	1.87		
		April 07, 2024	RMSE	2.32	2.66		
			St.dev	1.58	1.68		
		MEAN		3.30	4.09		

leading to a persistently erosive state throughout 2018. A partial recovery of the shoreline position was then recorded during 2019. However, the high standard deviation values observed in this area are indicative of significant statial variations, reflecting shoreline positive and negative fluctuations over medium time periods.

A more specific analysis in the medium-term period was represented

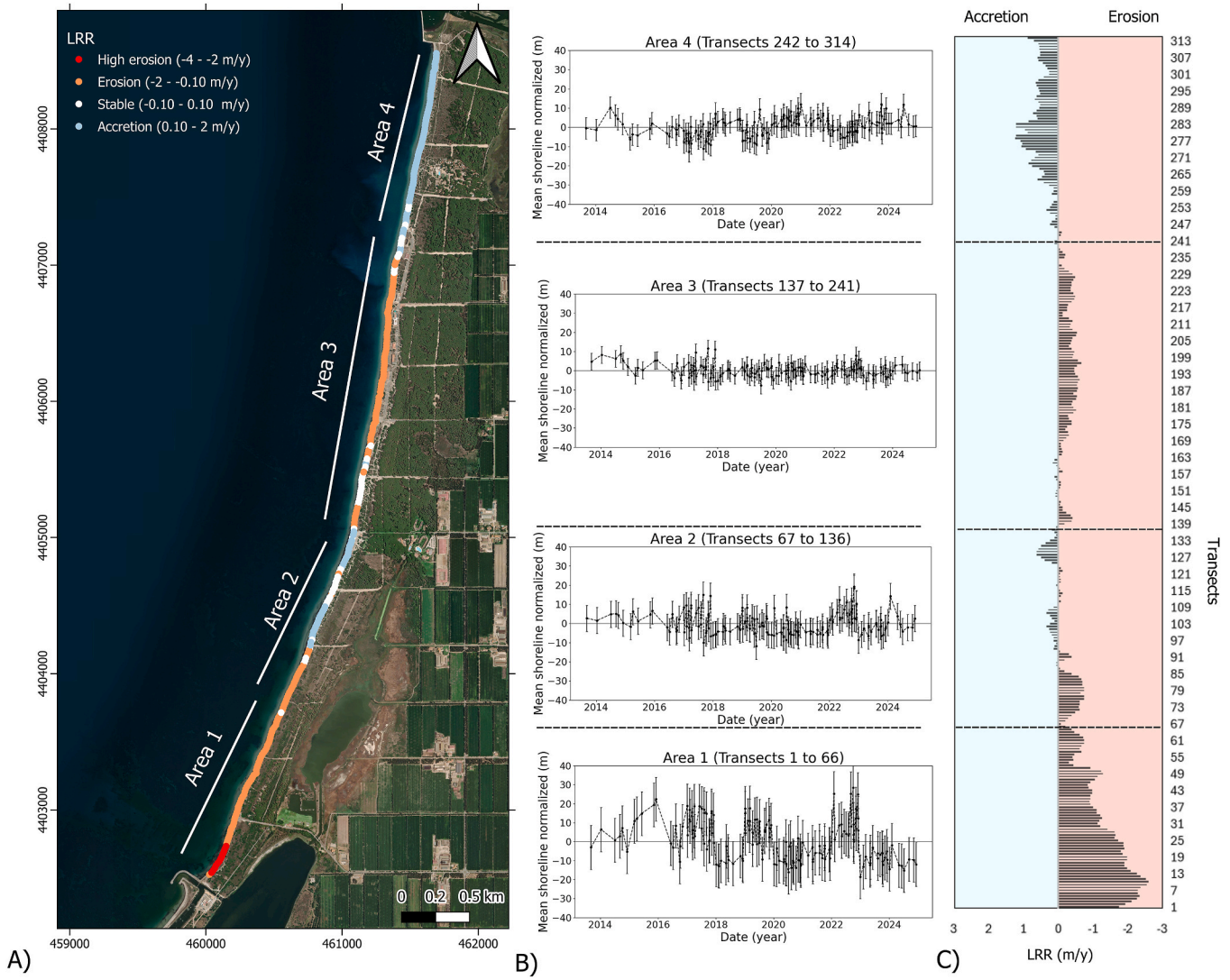

Fig. 6. Medium term analysis (2013–2024). Basemap google satellite; A) Map of Linear regression rate (LRR); B) Temporal Shoreline Position Anomaly, Normalized to the Historical Mean (2013–2024); C) Graphical visualization of LRR.

using the Hovmöller diagram (Fig. 7), which illustrates the individual shoreline movements extracted using SAET in the four areas. In the southern part of Arborea (Area 1), both erosional and accretionary trends are evident, with the latter being more prominent. Accretionary events often follow shortly after erosional episodes and can persist over extended periods, with erosional shifts ranging from −20 to −40 m and accretional movements spanning from +20 to +60 m. The Area 2 is generally characterized by stable conditions or slight erosion until the first half of 2017. Area 3, on the other hand, appears stable until 2015, after which it begins to show signs of erosion that do not seem to recover by 2024.

In contrast, the northern sector (Area 4) predominantly exhibits accretion, with an increasing frequency and intensity of shoreline advancement, reaching up to +40 m, towards the northernmost transects, particularly over transect 280. The periods during which Areas 1, Area 2 and 3 experienced the most significant erosion occurred between 2018 and 2019, 2020–2022, and 2023–2024. Notably, these same periods correspond to phases of accretion observed in Area 4.

Fig. 7A has been correlated with storm events that occurred during the selected time period (Fig. 7B), illustrating how the most intense storms typically trigger erosive responses across most areas, sometimes influenced by wave direction. For example, the storm on March 31, 2018, characterized by a peak wave height of 4.52 m and a southwest (SW) direction, caused shoreline retreat ranging from 5 to 40 m in Areas 1, 2, and 3, while Area 4 experienced accretion between 5 and 40 m. A similar pattern is observed throughout much of 2024, during which storms predominantly from the southwest also resulted in erosion of up to 40 m in Area 1 and accretion of up to 40 m in Area 4. Storm events occur more frequently during the winter months and many of these events are associated with a beach response, showing widespread erosion across most transects. The highest number of storm events occurred mainly in 2018 and 2019, while the most intense events were recorded in 2017, 2018, and 2023, with peak significant wave heights ranging between 6.5 and 7 m. The highest value overall was observed in February 2017, reaching 7.06 m Most storm events have an approach direction between 280 and 320°, although other events are also observed with approach directions ranging from 225 to 275°. In some cases, NW storms are followed by significant accretion in Area 1, as observed during the early months of 2022, when shoreline advancement reached nearly 60 m. In other instances, however, these events result in erosion even in Area 1, such as in early 2020 and 2023. Notably, Areas 1 and 4 exhibit a complementary dynamic, with erosion in one area often corresponding to accretion in the other, and vice versa.

3.4. Shoreline-dune toe interaction

The analysis of the evolution of the dune toe, as illustrated in Fig. 8, indicates In Area 1 the NSM reveals significant erosion of the dune toe in both the medium-term and long-term analyses, with values exceeding −20 m in the long-term analysis. In contrast, the northern part (Area 4) shows accretion, with values of about 20 m in both analyses, with higher values in the medium term. The southern area (Area 2) also shows evidence of erosion in the long-term analysis, with values reaching 20 m of retreat. In contrast, Area 3 is more balanced, displaying both erosion and accretion of the dune and shoreline in the long-term analysis. In the medium-term perspective, the dune tends to show accretion, while the shoreline remains more variable.

A comparison between the NSM calculated for the shoreline extracted from aerial photographs and using the SAET algorithm (SDS) and the NSM calculated for the dune toe from 2016 to 2024 reveals distinct patterns (Fig. 8B and C). The graphs are structured such that points falling within the red area indicate simultaneous erosion in both dune toe and shoreline, whereas points within the light blue area denote simultaneous accretion in both dune toe and shoreline. Grey areas

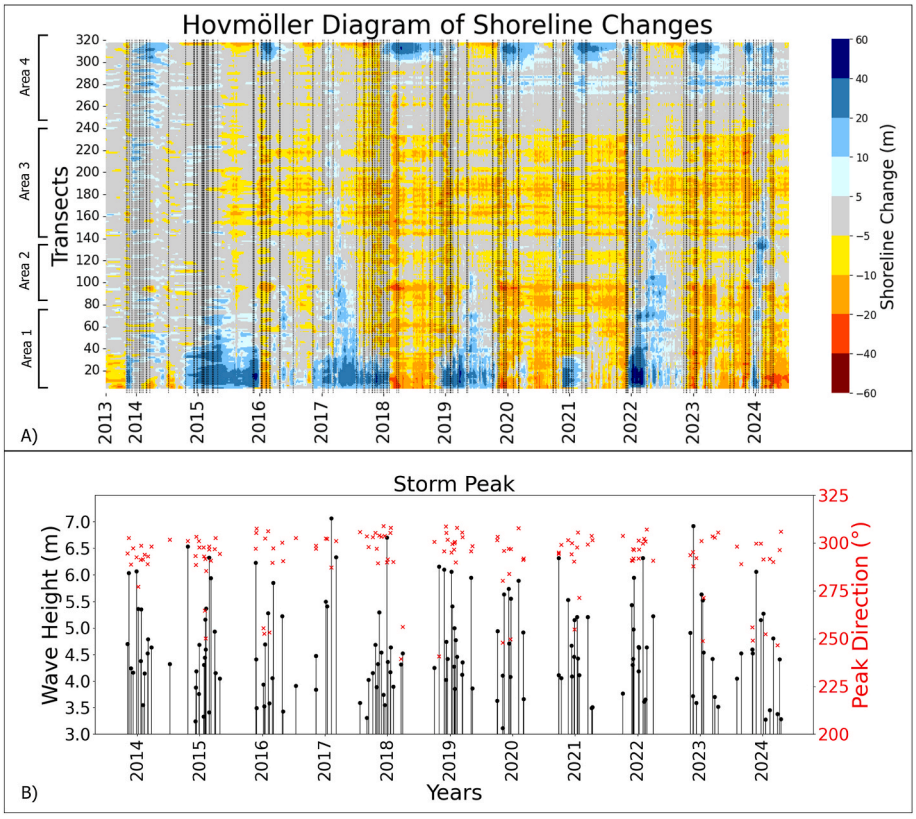

Fig. 7. A) Shoreline changes on Arborea beach relative to the average shoreline position in the first year, (dashed black lines corresponds to the storms peaks); B) Storm Peaks. The data was obtained from the Copernicus Marine Environment Monitoring Services (CMEMS); the selected point was located in the entrance of the Gulf of Oristano (coordinate point: 39.84 N, 8.39 E (EPSG:4 326)).

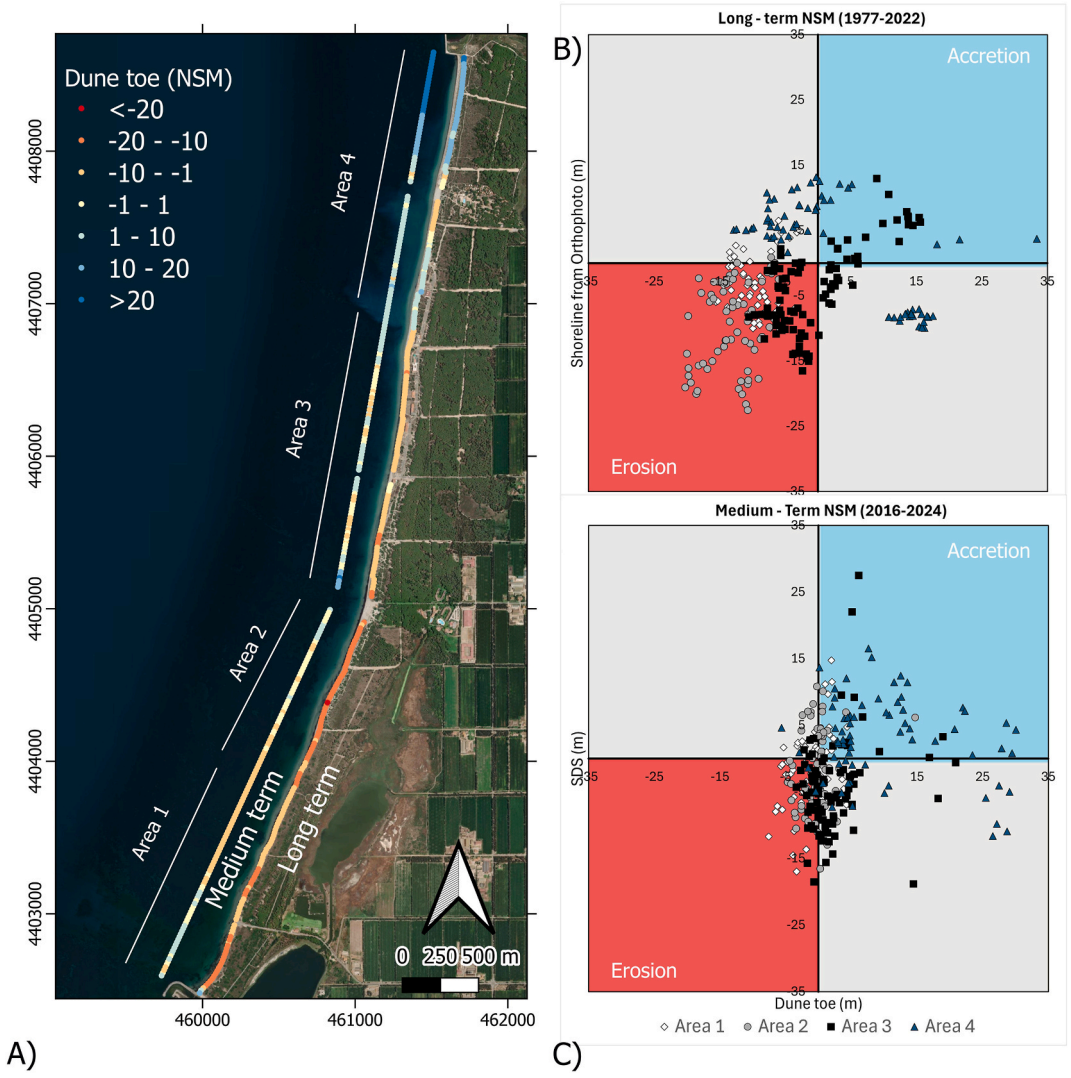

Fig. 8. – A) Net shoreline movement (NSM) from DSAS of the dune toe Long-term (1977–2022) and Medium-term (2016–2024). *Basemap google satellite*; B) Long-term NSM of the dune toe and shoreline displacement from 1977 to 2022; C) Medium-term NSM of the dune toe and SDS from 2016 to 2024.

represent non-uniform conditions, reflecting variability of the two analysed parameters in different directions (erosion/accretion). In Area 1, both the dune and the shoreline are eroding, except for some points that fall within the accretion zone, corresponding to the extreme southern part near the jetties. In Area 2, the trend is more variable, as some points fall within the red zone, indicating erosion of both the shoreline and the dune, while others fall within the blue zone, where accretion of both features has occurred. This pattern is particularly evident in the medium-term analysis, whereas in the long-term analysis, greater erosion is observed. In Area 4, by contrast, a more accretional pattern is observed for both the dune and the shoreline, especially in the medium-term analysis.

These trends may be explained by the subsequent local-scale analysis, conducted by examining, zone by zone, the hotspot areas where the dune toe experienced the most significant erosion. This is further evidenced in the analysis of the relationship between the dune toe and shoreline positions presented in Fig. 9. For this analysis, the density of shorelines that are located landward with respect to the oldest dune toe (refer to paragraph 2.7) during the period 2016–2022 was calculated to identify hotspot areas where shoreline position interact with dune toe. Notably, Fig. 9 shows that Area 1 presents regions with high line density during both the 2016–2018 and 2019–2022 periods. As a result, the cumulative contribution highlights elevated densities, especially in the northern part, along with a modest dune retreat response. This response appears to be more accurate and spatially consistent in the northern portion than in the southern part throughout the study period. Area 2 displays a similar pattern, with high densities distributed across nearly the entire area. In this case, a stronger correlation with dune movements is observed: erosion zones correspond to higher densities, while accretion zones align with low or absent densities. In Area 3, density values are lower overall, and during the 2016–2018 period the distribution appears more limited across the area. In the final cumulative contribution, the zones with higher density again correspond to dune retreat, whereas areas with lower or no density are associated with accretion. Finally, in Area 4, high density values are observed only in the northernmost portion and only during the 2016–2018 period. From 2019 to 2022, density is absent. In the total contribution, erosion is mainly detected in the northern area where high density is present, entirely as a result of the 2016–2018 data. Most of the area shows accretion, with isolated erosional spots that do not correspond to medium or high density values.

The analysis in Table 4, which correlates shoreline overpasses of the dune toe (average distance from the storm in our dataset of 2–3 days) with storm wave parameters, indicates that Areas 1 and 2 are the most

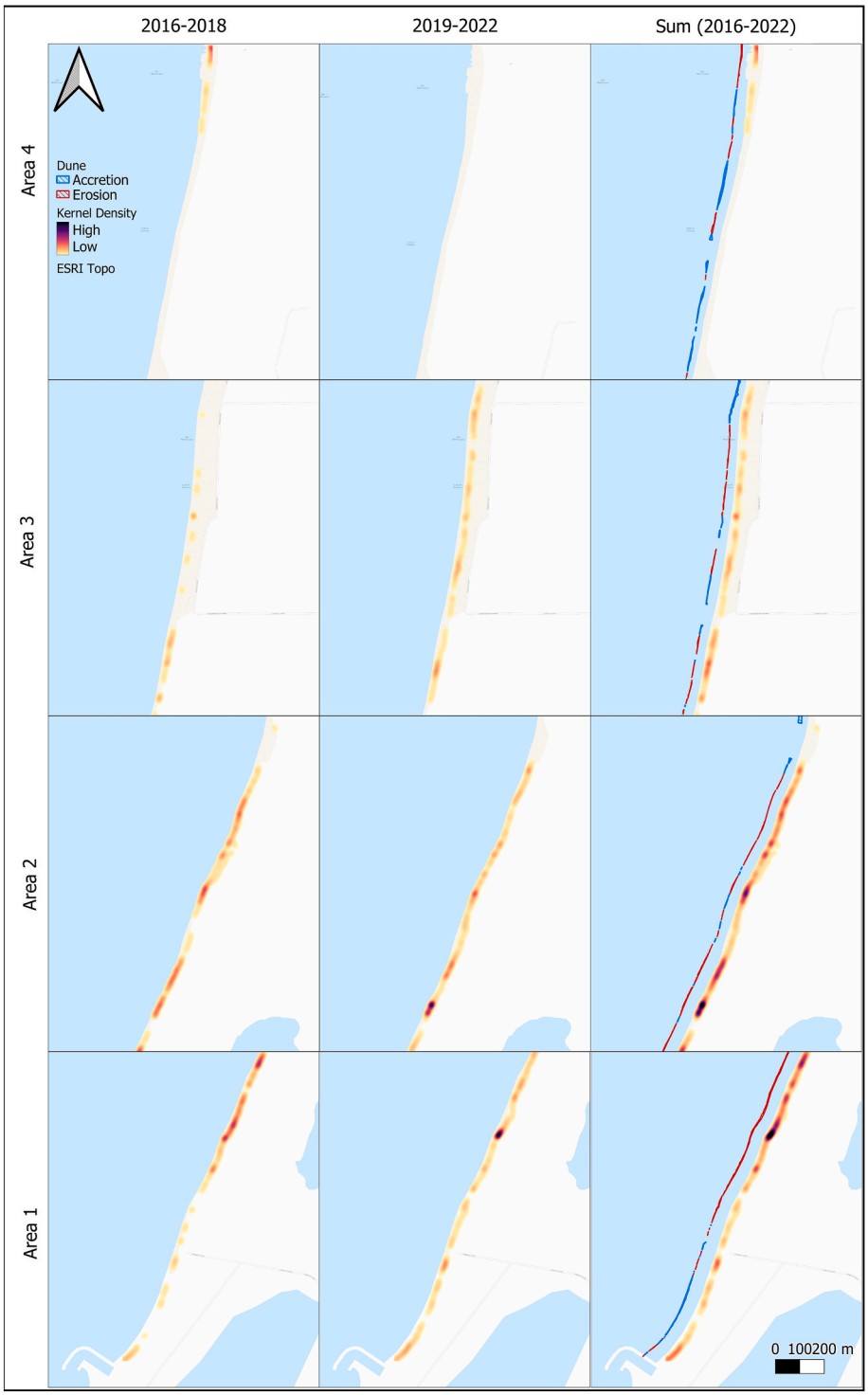

Fig. 9. – Analysis based on SDS and dune toe mapped on orthophotos. Kernel density of the SDS overpassing the oldest dune toe and dune toe migration from 2016 to 2022. The polygons represent the areas between the oldest and the most recent shoreline. Blue polygons show accretion; red polygons represent erosion (dune toe retreat).

frequently affected by overpass events. In contrast, overpasses in Areas 3 and 4 occur only up to 2018, after which the 2019 dune toe is adopted as the reference threshold. *Posidonia* in the form of active banquette is most commonly observed in Area 1, while it appears with moderate frequency in Areas 2 and 3. In Area 4, semi-active banquette is more frequently recorded. In many cases—particularly in Area 1—the presence of banquette is detected even prior to storm events. Its removal as a result of storms is observed only in two instances: in Area 2 during the event on March 07, 2017, November 13, 2017 and October 10, 2019, and in Area 3 during the event on November 20, 2020. The only events that do not result in *Posidonia* accumulation in Areas 1 and 2 but do trigger accumulation in Areas 3 and 4 are those of March 31, 2018; October 29, 2018; December 10, 2019; December 23, 2019; and February 04, 2020. The first two events recorded significant peak wave heights of 4.52 m

Table 4
Relationship between the presence/absence of Banquette and the overpass or non-overpass of the dune toe before and after storm events. The symbols correspond to Table 1.

Presence of posidonia	No presence of posidonia	No data	Overpass dune toe	No overpass dune toe	Area 1			Area 2			Area 3			Area 4		
Storm date	Wave Height Peak (m)	Wave period (s)	Wave direction (°)	Storm duration (hours)	Pre	Post	Over	Pre	Post	Over	Pre	Post	Over	Pre	Post	Over
07/03/2017	6.33	8.78	301	27												
25/07/2017	3.59	5.43	306	23												
03/09/2017	3.31	5.27	304	14												
11/09/2017	4.02	7.01	298	21												
06/10/2017	4.16	5.83	303	15												
23/10/2017	4.69	7.33	305	24												
29/10/2017	3.89	6.86	297	31												
06/11/2017	4.33	4.08	289	36												
13/11/2017	5.29	6.05	304	28												
03/02/2018	3.90	4.95	290	20												
31/03/2018	4.52	7.04	256	27												
29/10/2018	6.16	8.64	241	24												
09/01/2019	6.06	8.38	295	37												
03/02/2019	4.77	5.04	290	36												
11/02/2019	4.46	7.05	308	17												
14/03/2019	4.36	6.63	303	42												
03/10/2019	3.63	4.85	301	19												
07/10/2019	4.94	6.30	303	12												
10/12/2019	5.74	4.76	297	26												
23/12/2019	5.55	7.88	297	54												
04/02/2020	5.89	8.25	308	24												
07/03/2020	3.66	4.26	292	17												
20/11/2020	5.53	7.77	302	23												
07/04/2021	3.49	5.66	304	20												
06/10/2021	3.77	6.17	304	12												
11/12/2021	5.95	8.32	296	33												
02/04/2022	5.22	7.16	291	40												

and 6.16 m and are the only ones with peak wave directions originating from the southwest. The latter three events exhibited significant peak wave heights of 5.74 m, 5.55 m, and 5.89 m, respectively, and caused dune toe overpasses in Areas 1 and 2. Notably, the December 23, 2019 storm stands out as the longest-lasting event, with a duration of 54 h. Finally, it should be noted that overpass was observed in the presence of Posidonia prior to the storm on only four occasions throughout the entire dataset, and exclusively in Area 1.

4. Discussion

Long-term analysis (Fig. 4) provided insights into shoreline dynamics over a 68-year period, revealing opposite overall tendenciesbetween Area 1 and Area 4. In Area 1, erosion predominates, whereas in Area 4, a slight accretional trend is detected but not statistically significant. Specifically, between 1978 and 1997 (Fig. 4B), accretion was observed in Area 1 to the south, while erosion occurred in Area 4. This pattern corresponds to the period of construction of the two jetties connected to the adjacent lagoons, which have disrupted the sedimentary balance maintained by alongshore currents (Ranasinghe and Turner, 2006; Vaidya et al., 2015). As a result, the statistical parameters (R^2 and p-values) reflect the shoreline evolution that is characterised by varying trends that may depend both on anthropogenic interventions and on the natural behaviour of the beach itself, where frequent accumulations of *Posidonia oceanica* contribute to temporal variability. Therefore, the long-term trends should be interpreted as an indication of the overall behaviour of the different sectors, whereas the temporal evolution displayed in Fig. 4B more effectively represents the dynamics of Arborea

Beach. Indeed, comparing the first and last shorelines within the analysed time frame, an overall retreat of about 5 m is observed in Area 1, around 10–15 m in Areas 2 and 3, and an accretion of approximately 10 m in Area 4. However, during the intervening years, the shoreline positions fluctuated considerably, showing rather variable trends. In this context, the overall spatial behaviour described here aligns with the findings of Simeone et al. (2024), who documented similar shoreline developments in the same sector of the gulf. Looking at the satellite data, it became apparent that all four areas exhibit the same pattern of the long-term analysis, with the same trend of change but different magnitudes. In particular, the southern area (Area 1) shows an erosion rate of nearly −3 m per year, while Area 4 experiences an accumulation rate of almost +2 m per year. These higher medium-term rates, compared to the long-term periods could be attributed to two main factors. First, satellite imagery offers a higher temporal resolution than aerial photographs, resulting in a larger and more detailed dataset. As a consequence, medium-term shoreline changes related to the accumulation of banquette deposits are more clearly highlighted, a phenomenon that it is not detectable when solely relying on orthophotos. Second, the longer the time interval considered, the lower the displacement values tend to be, as the increased temporal coverage smooths out medium-term fluctuations (Dolan et al., 1991; Romine and Fletcher, 2013).

The error analysis results provide confirmation that the shoreline extracted by the algorithm effectively corresponds to the water–sand or water–banquette boundary (Table 3). Building on these findings, a comparative analysis of the shorelines extracted using different spectral indices and classification methods within SAET (Fig. 5), as well as a benchmark comparison against the widely used CoastSat tool, revealed critical differences in performance under varying environmental conditions (Table 3). Although both CoastSat and SAET were applied to the same set of satellite images, they were not configured using the same spectral index in the comparative analysis. Specifically, CoastSat was used with its default index, MNDWI, whereas SAET was configured with AWEInsh, as this index produced the lowest RMSE value in our tests. Despite this difference, the results still offer valuable insights into the relative performance of the two tools under the same environmental and temporal conditions. The MNDWI index, commonly used in shoreline extraction due to its ability to enhance water–land contrast by exploiting reflectance differences between the green and SWIR1 bands (Xu, 2006), demonstrated moderate accuracy when applied via CoastSat. In this case, the RMSE against the GPS-derived instantaneous water line reached values as high as 16.79 m (mean RMSE: 13.62 m), and even higher when compared to the Wet/Dry line reference (mean RMSE: 18.40 m). In contrast, SAET achieved markedly lower errors using the AWEInsh index (mean RMSE: 3.30 m against the instantaneous water line, 4.09 m against Wet/Dry line), confirming its better suitability for conditions characterized by dark, shadowed surfaces such as *Posidonia* banquettes. Its stability therefore made it the most appropriate index for medium-term analyses encompassing a range of conditions. Additional analyses supporting these results are presented in the Appendix (Figures A1–A2 and Table A1 including plots with the differences between the surveyed shoreline and SDSs, Q–Q plots and bias values. These complementary results clarify that the AWEInsh achieves lower RMSE values and greater geometric consistency with the GNSS reference shoreline. In contrast, AWEIsh index (Feyisa et al., 2014), optimized for detecting water in shadowed environments, although exhibits a more symmetric distribution of residuals (Q–Q plots), performed poorly in presence of banquette, with frequent overestimation of water-covered areas due to the spectral similarity between dark organic matter and water. This led to shoreline displacements of several meters landward (as shown in Figure A 1), as the algorithm misclassified the *Posidonia* as open water. Conversely, AWEInsh, designed for scenes without significant shadowing, demonstrated improved robustness in clearer coastal conditions and showed relatively low RMSE values in cases where banquette presence was limited (Feyisa et al., 2014). The K-means approach yielded variable results: while it could accurately capture shorelines in scenes with high spectral contrast, its unsupervised nature and lack of context sensitivity made it unreliable in complex beach environments (Yilmaz, 2023), particularly where *Posidonia* was present or pixel mixtures were common. MNDWI (Xu, 2006) displayed higher RMSE and greater variability, particularly during periods of high *Posidonia* coverage (e.g., May 26, 2023 and February 15, 2024), where shoreline extraction errors reached up to several meters. In these cases, the spectral similarity between moist *Posidonia* wrack and water likely contributed to overestimation of the water extent, shifting the shoreline landward. This supports the interpretation that, despite its widespread use, MNDWI may not adequately distinguish between water and dark vegetative material without further refinement or context-specific adjustment. These differences between CoastSat and SAET likely stem not only from the indices used but also from fundamental methodological distinctions. CoastSat's fully automated workflow includes a global thresholding strategy and subpixel contour fitting that may oversimplify complex shoreline textures and spectral transitions. Moreover, the automatic co-registration of satellite scenes in Google Earth Engine, while generally reliable, may introduce spatial offsets when images from different sensors or acquisition geometries are not perfectly aligned, possibly contributing to the consistent seaward displacement observed in CoastSat-derived shorelines (Vos et al., 2019). In contrast, SAET allows for index selection, adaptive thresholding, and supports the use of precisely georeferenced input data maintaining official coordinate reference systems (CRS) (Palomar-Vázquez et al., 2023). These features contribute to its better performance in capturing shoreline positions under spectrally and spatially heterogeneous conditions, such as those influenced by *Posidonia* accumulations. Importantly, all extraction methods showed closer agreement with the GNSS RTK shoreline in the absence of *Posidonia*, confirming that *Posidonia banquette* presence plays a significant role in degrading the accuracy of spectral shoreline extraction (Caldareri et al., 2024). These findings highlight the importance of carefully selecting both the spectral index and the processing method according to site-specific conditions. Such an evaluation allows for a better understanding of the associated errors and ensures that the most suitable approach is applied before undertaking large-scale shoreline extraction. Focusing on the medium-term analysis, it is noticeable that the high temporal resolution has allowed the identification of some fluctuations in the shoreline, particularly in Areas 1 and 4. Moreover, the calculated error is well below the pixel resolution of the satellite imagery used, which increases the reliability of the shoreline shifts, as their magnitude exceeds the error threshold (Vos et al., 2023a,b). In Area 1, for example, large accumulations are observed, often interrupted abruptly by erosional events, followed by a subsequent strong accumulation (Fig. 7A). These mostly coincide with storm events that cause significant erosion (Fig. 7B). As this area is particularly prone to substantial *banquette* accumulation, significant accretion events could be associated with the formation of *banquettes* following storm events. However, although according to (Gómez-Pujol et al., 2013) *Posidonia banquettes* do not remain stable over long periods, our results show accretion that appear to persist for several months. Based solely on shoreline observations, it is not possible to determine whether these accretion phases correspond exclusively to the accumulation of banquettes or if they result from actual sediment accretion. One possible hypothesis is that banquettes initially accumulate, and are subsequently covered by sand due to wind action and wave run-up (Vacchi et al., 2017). This phenomenon was observed by (Trogu et al., 2023) in the Poetto beach, where monitoring showed that, under calm conditions, *Posidonia banquettes* were covered by sediments within a few days due to the influence of offshore winds. This may represent a limitation of this type of methodology, but it could be mitigated by incorporating additional data such as *in situ* observations (e.g., topographic information derived from UAV or LiDAR surveys) or high-resolution imagery (e.g., PlanetScope) to determine whether short-term changes are driven by banquette fluctuations or by sediment dynamicsThis could be complemented by analyses based on freely available multispectral or

hyperspectral satellite products, using either visual interpretation or classification approaches.Moreover, the strong irregularity of the data in the area affected by the presence of banquettes makes evolutionary analysis particularly complex, producing trends that, due to high SDS fluctuations and elevated standard deviation values, exhibit limited reliability when attempting to perform rate-based analyses. This is particularly evident in Fig. 6C, where the LRR in Area 1 displays an erosive trend, whereas Fig. 6B shows a pattern lacking a clear directional tendency but characterized by rather significant variations. The variability observed highlights how beaches influenced by *Posidonia oceanica* banquettes can display highly dynamic behaviour, where the deposits become part of the coastal system and act as natural components, contributing to its morphological variability (Astudillo-Gutierrez et al., 2025). It is also important to note that annual rates should be interpreted with caution, since their magnitude is of the same order as the calculated error (2–3 m), which may mask or exaggerate annual variations. However, given that the analysis covers a 10-year period, these uncertainties are largely absorbed within the overall trend, supporting the robustness of the medium-term shoreline dynamics.

Regarding fluctuations in the dune toe position, the analysis (Fig. 8) generally revealed greater erosion in the southern and central-southern areas (Area 1 and Area 2) over both the medium and long-term, while accretion was observed in the northern area (Area 4). When analysing the shoreline-dune toe interactions (Fig. 9), it is evident that the zones with the highest kernel density, i.e., the hotspot areas, correspond to those where actual dune erosion occurred. This may suggest that these zones were particularly affected by repeated shoreline retreat, and that there is a good relationship between the number of shoreline overpasses and dune toe retreat. Indeed, areas with low or no kernel density showed limited retreat or even accretion of the dune toe. This accretion may be also attributed to the presence of *Posidonia oceanica* berms and associated Neptune balls, which, after being deposited at the base of the dune, can facilitate vegetation regrowth and contribute to the stabilization and reinforcement of the embryonic dune system (Del Vecchio et al., 2017; Jiménez et al., 2017; Menicagli et al., 2024). The presence of *Posidonia* in the form of banquettes is neither spatially nor temporally consistent across the study area. The results of the analysis (Table 4) examining storm parameters and the presence or absence of *banquette* before and after storm events, confirm that its distribution is variable, yet follows certain patterns (Fernandez-Mora et al., 2025). In most cases, *Posidonia* tends to be more abundant following storms, which aligns with the theory proposed by Gómez-Pujol et al. (2013). However, it is generally concentrated in Areas 1, 2 and 4. This suggests that these three areas act as depositional traps, allowing for longer retention of *Posidonia* material. In Area 4, *Posidonia* is almost always present, both before and after storm events, whereas in Areas 1 and 2, its presence tends to fluctuate more significantly. Area 4 also shows the least overpassing of the dune toe and, according to all previous analyses, is the area most subject to accretion rather than erosion. This may be due to the presence of *Posidonia*, which in turn could be influenced by the predominant direction of storm waves, primarily from the northwest, and the presence of the jetties, which promotes nearshore accumulation through wave refraction (Vaidya et al., 2015). Only two events originated from the southeast within the observed time series, and both promoted the accumulation of *Posidonia* towards Area 3 and 4, confirming that Area 4 is fed by more than one wind direction. In fact, during Libeccio events, longshore transport in this area moves from south to north, while during Mistral events it moves from north to south, creating a vortex zone between the inner part of the gulf and Frasca cape (southern cape)(Cucco et al., 2006). Moreover, according to the data in Table 4, this Area 4 is also less affected by dune toe overpassing events. During these two southeast events, overpassing occurred only when wave height reached 6.16 m and did not affect Area 4. Altogether, this appears to support the interpretation that Area 4 functions as a sediment and *Posidonia* accumulation zone, which would explain the accretion consistently observed across all analyses. In contrast, Area 1 appears to be more variable and is more frequently exposed to dune toe overpassing events, even when Posidonia banquettes are occasionally present before the storm. This is likely due to its orientation, which allows storm waves to impact the area more directly. Nevertheless, the presence of the jetty still promotes occasional accumulation events, although these tend to persist for a much shorter duration compared to Area 4, resulting in banquettes that are less stable, more fragmented, and consequently more mobile. This may be due to the presence of the jetty itself, which facilitates the formation of an offshore-oriented scour channel enhancing the transfer of sediment and *Posidonia* debris away for the shoreface. In the map of *Posidonia oceanica* distribution (Simeone and De Falco, 2013) indeed, it can be observed that this area a less dense *Posidonia* meadow compared to the other zones, and that there is a section near the jetty where it is completely absent. The absence of *Posidonia oceanica* on the seabed may indicate that the area is subject to strong wave-driven currents, which prevent the establishment of seagrass meadows that typically grow under moderate wave energy conditions (Boudouresque et al., 2012). Moreover, according to (De Grissac and Boudouresque, 1985), the disappearance of the meadow could lead to shoreline retreat by reducing wave attenuation, destabilizing sediments and disrupting the balance of sediment circulation, potentially leading to net sand loss. In Area 4, a significant advancement of the dune toe, exceeding 30 m, was observed (Fig. 10), likely driven by the frequent and almost stationary accumulation of *Posidonia*, as previously discussed and illustrated in Fig. 8. Specifically, no *Posidonia* was present on the beach in 2006 (Fig. 10A), while the 2010 orthophoto (Fig. 10B) reveals an accumulation approximately 20 m wide, which later transformed into a progressively accreting dune toe visible in the 2022 image (Fig. 10C). According to the banquette classification, there has therefore been a transition over time from an active banquette condition to a stable one (Table 1). This evolution is also reflected in the position of the military bunker: in 2006 it was located close to the shoreline, while in 2022 it appears embedded within the newly formed dune. The same can be seen in the image from April 06, 2025 (Fig. 10E), where the bunker is visible, surrounded by vegetation. The photograph taken in April 2025 further documents the current state of the beach, showing the boundary between the old and new dunes now fully covered by vegetation (Del Vecchio et al., 2013) (Fig. 10D). Although the area was subject to dune toe overpassing events until 2018 — as confirmed by the kernel density analysis (Fig. 9)— It is possible that the area was no longer significantly reached by the shoreline in subsequent years, and that the presence of well-established vegetation and long-term accretion, identified in the previous analysis, helped to mitigate storm impacts (Fernández-Montblanc et al., 2020), making the area naturally more protected.

Moreover, it was observed that this area has never been subject to *Posidonia* removal. In fact, since these beaches are not entirely pristine but experience moderate to low tourist pressure, they are also sometimes affected by cleaning interventions aimed at removing *Posidonia oceanica* debris. There is limited documentation confirming the actual removal of *Posidonia oceanica* banquettes from the beach. However, evidence of these interventions exists through the social media page of the company responsible for beach cleaning (Società Cooperativa ECO.RI.SA. (Ecologia Risanamento Sardegna), 2015), which has documented the operations carried out. These data were therefore used to compare the previously analysed dune toe fluctuations with beach cleaning interventions. In this case, the areas were subdivided based on beach access points and subsequently grouped into three zones to facilitate interpretation. Fig. 11 presents the number of interventions and their relationship with dune toe variations, analysed using the NSM statistic. The image shows that areas where the highest number of interventions took place did not experience significant changes in the dune toe between 2013 and 2024. In some cases, dune accretion was even observed. This may be due to two factors: first, major dune removal interventions were carried out before the study period, for instance in the areas near access 12 and 13, from orthophoto can be observed that approximately 40 m^2 of dune was removed due to the construction of tourist resorts and

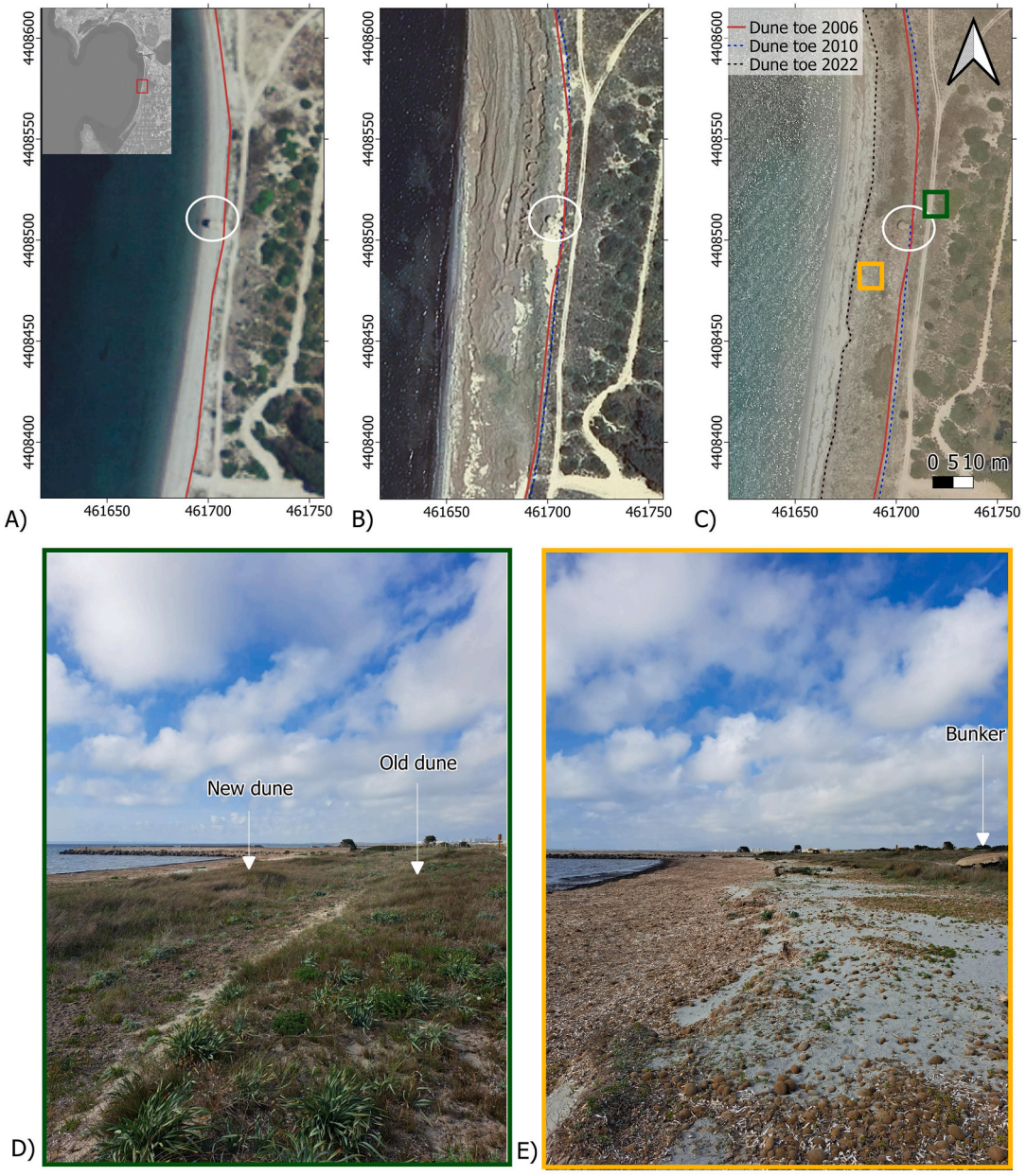

Fig. 10. – Dune accretion from 2006 to 2022 The white circle indicates the position of the bunker; (A–C) Orthophotos from 2006, 2010 and 2022 (Regione Autonoma della Sardegna, 2025); D) Picture of April 06, 2025 showing old and new dune (green square); E) Picture of April 06, 2025 showing the position of the bunker (orange square).

beach facilities between 2006 and 2010; second, during cleaning operations, the procedure involves depositing the removed material in the dune area, which may have contributed to dune protection and growth (Menicagli et al., 2024). This raises the question of whether the management practices used in places like Alghero (Manca et al., 2013)—such as putting the banquette back on the beach after removing it in the summer—might actually interfere with the natural regeneration process, which, as we have observed, requires the banquette to remain on the shore for longer periods. Moreover, these operations are mainly carried out before the summer season, during which less storm events are recorded (Martzikos et al., 2021). It is therefore possible that the frequent deposition of banquettes during the winter may have acted as a protective buffer for the dunes.

5. Conclusions

This study highlights the value of remote sensing for monitoring coastal dynamics and the morphological evolution of *Posidonia oceanica* banquettes. It represents one of the first comprehensive efforts to track the formation, persistence, and removal of these deposits across both medium- and long-term timescales via satellite datasets and to directly link these patterns to storm events. The findings demonstrate how storm direction and intensity influence banquette deposition and removal patterns across different sections of the beach. Our results indicate that frequent *Posidonia* accumulations, when persisting over long periods and evolving from semi-active to stable states, can act as effective natural barriers, protecting the shoreline and the dune toe from erosion. In contrast, when *Posidonia* remains on the shore only temporarily, its protective function on coastal dynamics appears to be reduced.

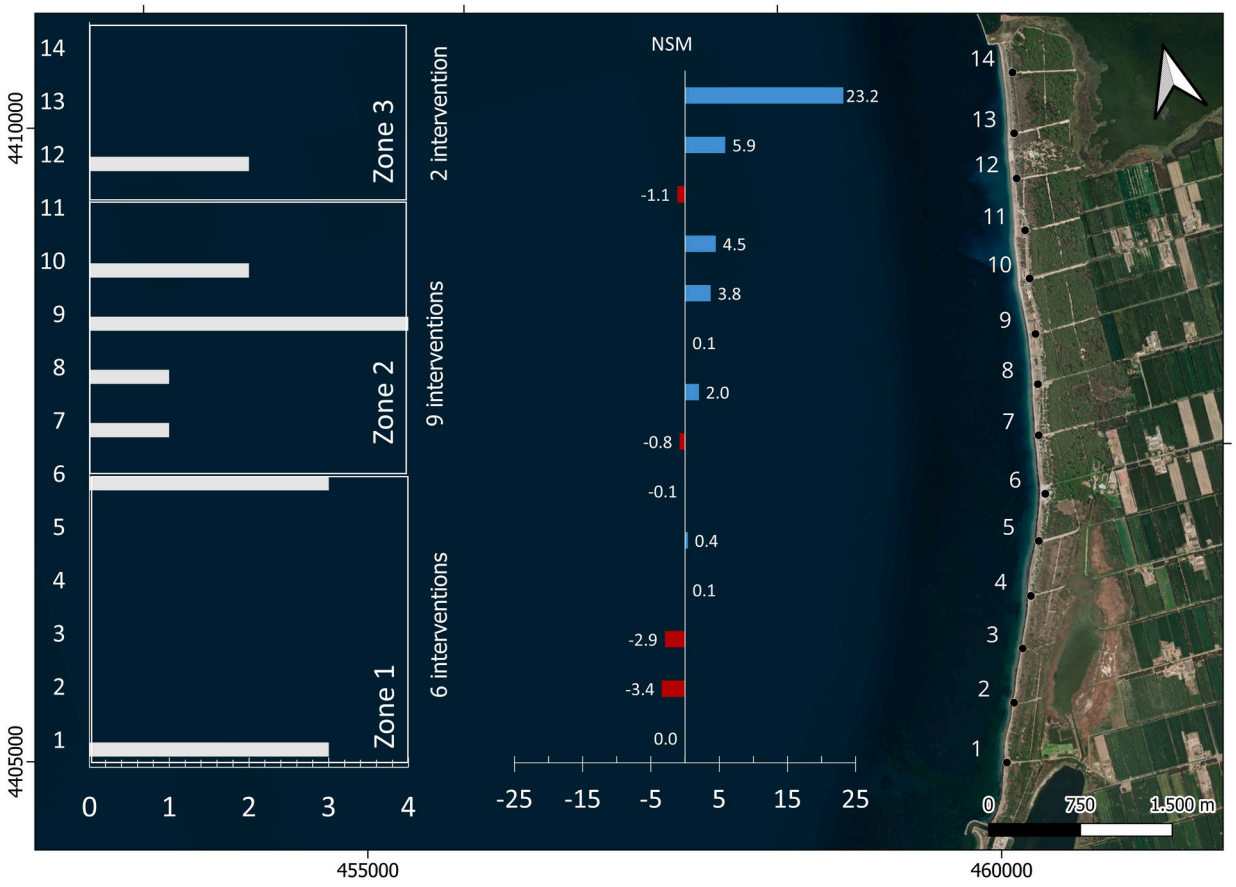

Access	1			2	3	4	5	6			7	8	9				10		11	12		13	14
Year of intervention	2018	2020	2024	/	/	/	/	2020	2023	2024	2020	2020	2013	2014	2015	2020	2018	2020	/	2023	2024	/	/
Number of intervetions	3			0	0	0	0	3			1	1	4				2		0	2		0	0

Fig. 11. – Number of cleaning interventions of the seagrass from the beach related to NSM of the dune toe from 2013 to 2024.

Moreover, their presence appears to support natural processes such as sediment redistribution and vegetation colonization, thereby enhancing dune resilience. However, human interventions, particularly beach cleaning operations, can inhibit vegetative regrowth and hinder dune stabilization. Additionally, the comparative evaluation of shoreline extraction methods underscores the importance of selecting appropriate spectral indices and classification techniques, especially in environments influenced by dark organic deposits such as *Posidonia* deposit. Further research should aim to refine shoreline extraction under these challenging conditions, which are common in many coastal settings. From a methodological perspective, comparing two independent limits, i.e., the instantaneous water line (water–banquette boundary) and the banquette–sand boundary corresponding to the landward edge of the accumulation, could help better understand the contribution of banquette to shoreline dynamics. However, current semi-automatic extraction algorithms cannot properly identify this second limit due to the spectral heterogeneity of the banquette, which remains a key challenge for future developments. The main limitations of this study relate to the spatial and temporal resolution of the satellite imagery. Higher temporal resolution would allow for more frequent observations, improving the tracking of short-term events and dynamic processes. Similarly, increased spatial resolution would enable more accurate interpretation of banquette morphology (especially its width across the beach) and facilitate finer-scale mapping of the dune toe, leading to more precise and consistent monitoring. Finally, this approach could be applied in areas with similar coastal settings, such as low-tidal, wave-exposed sandy coasts where *Posidonia oceanica* deposits exhibit some degree of persistence, as found along the Mediterranean coasts. In contrast, the applicability of this framework may be limited in environments characterised by large tidal ranges, which generally reduce the accuracy of SDS, mixed sediment compositions, or very small and short-lived wrack accumulations. Nevertheless, this research can serve as a valuable reference for future studies and applications in other regions where where seagrass or other debris deposits on the shore and interact with the beach-dune system.

CRediT authorship contribution statement

S. Terracciano: Writing – review & editing, Writing – original draft, Visualization, Validation, Methodology, Investigation, Formal analysis, Data curation, Conceptualization. **J. Montes:** Writing – review & editing, Writing – original draft, Visualization, Validation, Methodology, Investigation, Formal analysis, Data curation, Conceptualization. **R. Brunetta:** Writing – review & editing, Writing – original draft, Visualization, Validation, Methodology, Investigation, Formal analysis, Data curation, Conceptualization. **P. Cabrita:** Writing – review & editing, Writing – original draft, Data curation. **P. Ciavola:** Writing – review & editing, Writing – original draft, Visualization, Supervision, Resources, Project administration, Methodology, Funding acquisition. **C. Armaroli:** Writing – review & editing, Writing – original draft, Visualization, Methodology, Conceptualization.

Funding

This work is a contribution to the OVERSEE Project, financed by ASI under contract 2022-14-U.0. and PNRR-DM351 grant to the EMAS PhD program. P. Ciavola acknowledges the support of the University of Ferrara through the FAR 2023, 2024 and 2025 funding scheme.

Declaration of competing interest

The authors declare that they have no known competing financial interests or personal relationships that could have appeared to influence the work reported in this paper.

Acknowledgement

The authors acknowledge the support of the staff of the CNR-IAS institute for providing access to local GPS corrections and logistical support. They also thank Dr. Antonis Chatzipavlis, Dr. Enrico Duo, Dr. Juan Pedro Carbonell-Rivera and Dr. Stefano Fabbri for their support during the field data collection activities. Juan Montes was supported by a postdoctoral contract (DGP_POST_2024_00910) funded by Junta de Andalucía /CUII and FSE+.

Appendix

Table A.1
– Statistical parameters of the indices and classification methods of SAET algorithm.

Date	Error	MNDWI (m)	AWEIsh (m)	AWEInsh (m)	Kmeans (m)	Minor error (m)	Index	*Seagrass berm*
May 26, 2023	RMSE	3.96	1.97	3.98	1.87	1.87	Kmeans	Semi-active
	St.dev	1.97	1.09	2.14	1.06			
	Bias	3.37	0.89	3.40	−0.35			
October 10, 2023	RMSE	4.73	7.76	3.73	7.86	3.73	AWEInsh	Dispersed debris
	St.dev	1.38	2.04	2.03	1.81			
	Bias	−4.57	−7.37	−2.94	−7.62			
February 15, 2024	RMSE	3.40	4.02	3.28	5.51	3.28	AWEInsh	Active
	St.dev	2.06	2.65	1.88	1.49			
	Bias	2.35	2.35	2.90	5.44			
April 07, 2024	RMSE	4.89	6.43	2.32	3.23	2.32	AWEInsh	Absent
	St.dev	1.65	1.62	1.29	1.56			
	Bias	−4.52	−6.19	−1.20	−2.67			

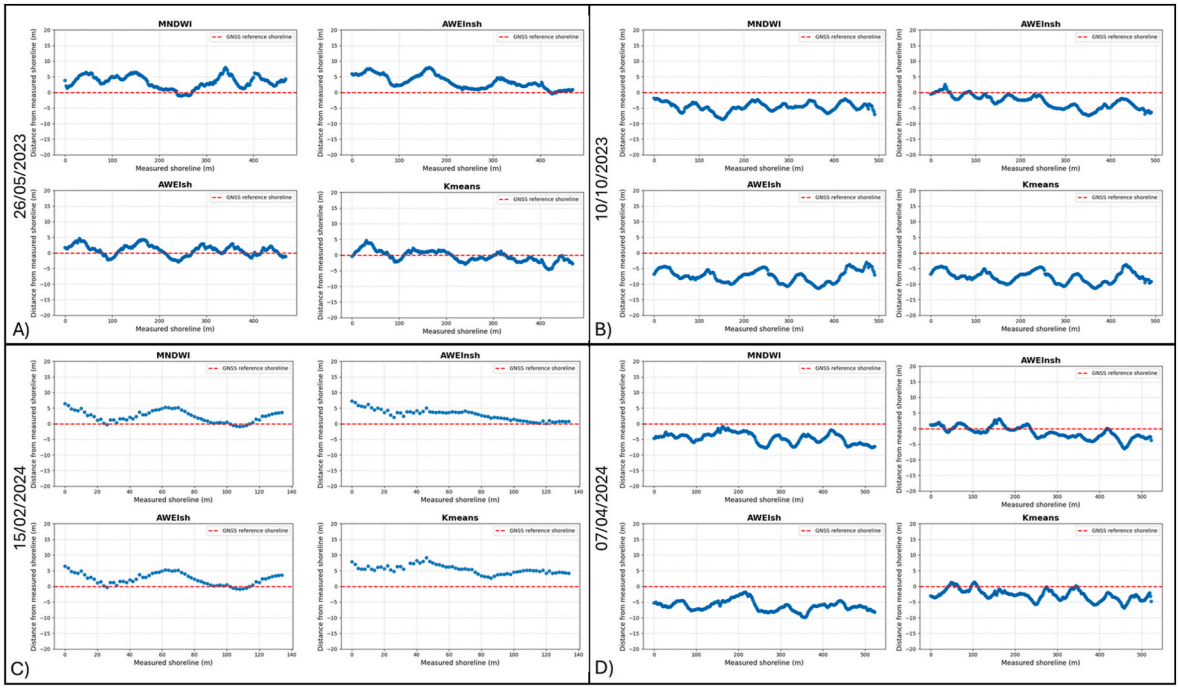

Fig. A 1. Plots of positive and negative distances between the GNSS reference shoreline (red dashed line) and satellite-derived shorelines obtained using different spectral indices (MNDWI, AWEInsh, AWEIsh) and K-means classification for four survey dates: A) 26/05/ 2023, B) October 10, 2023, C) 15/02/ 2024, and D) April 07, 2024. Each plot shows the distribution of perpendicular offsets along the measured shoreline with respect to the GNSS reference. This figure complements Fig. 5 and the summary statistics reported in Table A.1.

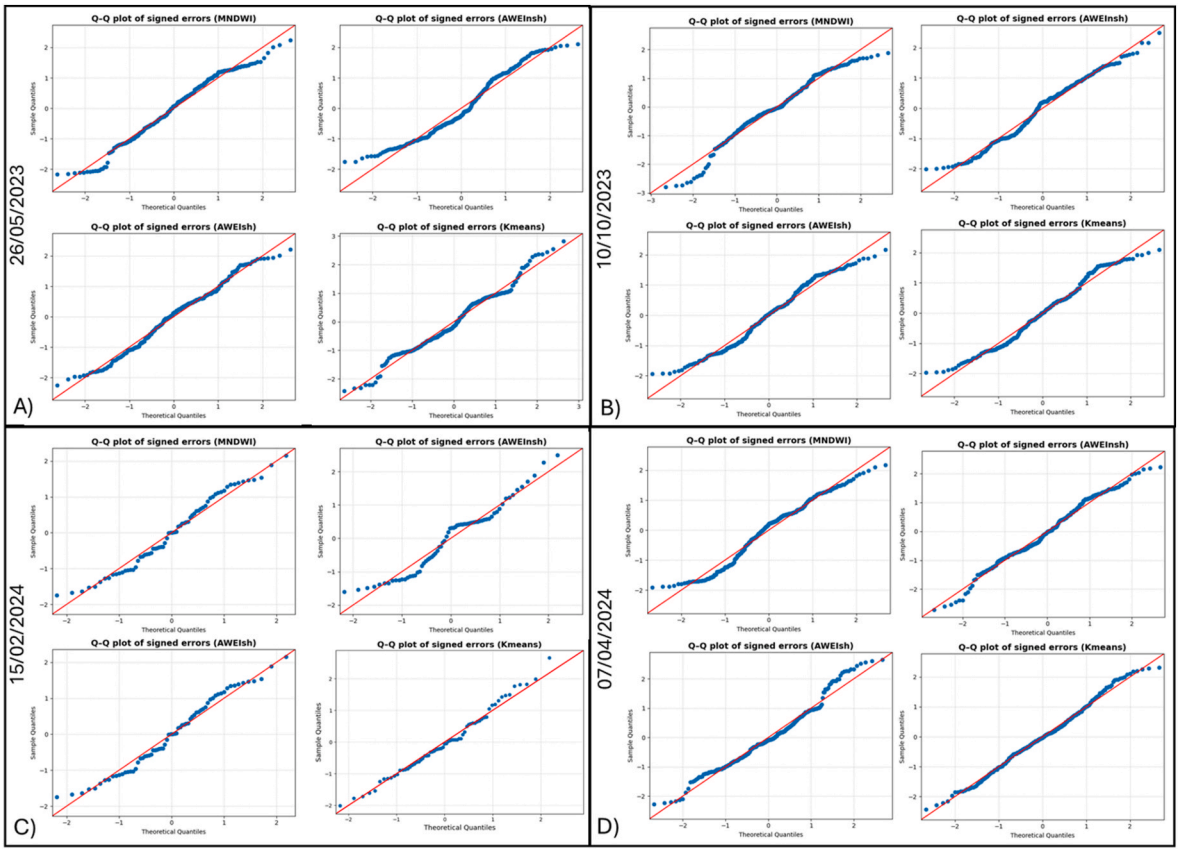

Fig. A 2. Q–Q plots of positive and negative shoreline displacement obtained comparing the GNSS reference line with satellite-derived shorelines (SDS) obtained using different spectral indices (MNDWI, AWEInsh, AWEIsh) and K-means classification for four survey dates: A) 26/05/ 2023, B) October 10, 2023, C) February 15, 2024, and D) April 07, 2024. This figure complements Fig. 5 and the summary statistics reported in Table A.1.

Data availability

The satellite data used in this study are freely available from the following sources.•

Sentinel-2 imagery: Copernicus Open Access Hub (https://dataspace.copernicus.eu/explore-data/data-collections/sentinel-data/sentinel-2)•

Landsat 8 and 9 imagery: USGS EarthExplorer (https://earthexplorer.usgs.gov/)•

CMEMS wave and sea-level products: Copernicus Marine Service (https://marine.copernicus.eu/)

The SAET (Shoreline Analysis and Extraction Tool) algorithm used for shoreline detection is openly available at: https://github.com/jpalomav/SAET_master: https://zenodo.org/records/10256957.

In addition to the openly available data listed above, field datasets are part of the main author's PhD thesis, currently under submission. Upon completion of the PhD program, they can be made available upon reasonable request to the main author.

References

Arriaga, J., Medellin, G., Ojeda, E., Salles, P., 2022. Shoreline detection accuracy from video monitoring systems. J. Mar. Sci. Eng. 10, 95. https://doi.org/10.3390/jmse10010095.

Astudillo, C., Gracia, V., Sierra, J.P., Cáceres, I., Sánchez-Arcilla, A., 2023. Posidonia beach-cast and banquette: evaluation of sediment trapping and characterisation for coastal protection. In: Coastal Sediments 2023. World scientific, pp. 2265–2277. https://doi.org/10.1142/9789811275135_0208.

Astudillo-Gutierrez, C., Gracia, V., Cáceres, I., Sierra, J.P., Sánchez-Arcilla, A., 2024. Influence of seagrass meadow length on beach morphodynamics: an experimental study. Sci. Total Environ. 921. https://doi.org/10.1016/j.scitotenv.2024.170888.

Astudillo-Gutierrez, C., Pavo-Fernandez, E., Gracia, V., Sierra, J.P., Llull, T., Mosso, C., Sanchez-Artus, X., Sanchez-Arcilla, A., 2025. Posidonia oceanica banquette accumulations in southern Catalonia: management approaches and key parameters for coastal protection. Front. Mar. Sci. 12. https://doi.org/10.3389/fmars.2025.1681826.

Boak, E.H., Turner, I.L., 2005. Shoreline definition and detection: a review. J. Coast Res. 214, 688–703. https://doi.org/10.2112/03-0071.1.

Boudouresque, C.-F., Bernard, G., Bonhomme, P., Charbonnel, E., Diviacco, G., Meinesz, A., Pergent, G., Pergent-Martini, C., Ruitton, S., Tunesi, L., 2012. Protection and conservation of Posidonia oceanica meadows, 202. https://doi.org/10.34894/VQ1DJA.

Briceño de Urbaneja, I.C., Pardo-Pascual, J.E., Cabezas-Rabadán, C., Aguirre, C., Martínez, C., Pérez-Martínez, W., Palomar-Vázquez, J., 2024. Characterization of multi-decadal beach changes in Cartagena Bay (Valparaíso, Chile) from satellite imagery. Remote Sens (Basel) 16, 2360. https://doi.org/10.3390/rs16132360.

Cabezas-Rabadán, C., Pardo-Pascual, J.E., Palomar-Vázquez, J., Cooper, A., 2025. A remote monitoring approach for coastal engineering projects. Sci. Rep. 15, 2955. https://doi.org/10.1038/s41598-025-86485-y.

Cabrita, P., Brunetta, R., Montes-Pérez, J., Terracciano, S., Duo, E., Ciavola, P., Armaroli, C., 2024. One-year evolution of a Mediterranean sandy beach with Posidonia oceanica banquettes (Arborea, Sardinia, Italy). Proceedings of the Tenth International Symposium: Monitoring of Mediterranean Coastal Areas: Problems and Measurement Techniques, Livorno (Italy) 11-13 June 2024. Firenze University Press, pp. 671–682. https://doi.org/10.36253/979-12-215-0556-6.58.

Caldareri, F., Sulli, A., Parrino, N., Dardanelli, G., Todaro, S., Maltese, A., 2024. On the shoreline monitoring via earth observation: an isoradiometric method. Remote Sens. Environ. 311. https://doi.org/10.1016/j.rse.2024.114286.

Corbí, H., Riquelme, Adrián, Megías Baños, C., 2018. 3D Morphodynamic modelling of a western Mediterranean beach with Posidonia oceanica banquettes using Terrestial Lidar. ISPRS Int. J. GeoInf. https://doi.org/10.3390/ijgi7070234.

Cucco, A., Perilli, A., De Falco, G., Ghezzo, M., Umgiesser, G., 2006. Water circulation and transport timescales in the Gulf of Oristano. Chem. Ecol. 22. https://doi.org/10.1080/02757540600670364.

Darwish, K.S., 2024. Monitoring coastline dynamics using satellite remote sensing and geographic information systems: a review of global trends. Catrina: Int. J. Environ. Sci. 31 (1), 1–23. https://doi.org/10.21608/cat.2024.233931.1196.

De Falco, G., Simeone, S., Baroli, M., 2008. Management of beach-cast Posidonia oceanica seagrass on the island of Sardinia (Italy, Western Mediterranean). J. Coast Res. 24, 69–75. https://doi.org/10.2112/06-0800.1.
De Grissac, J., Boudouresque, C.F., 1985. Rôles des herbiers de phanérogames marines dans les mouvements des sédiments côtiers: Les herbiers à Posidonia oceanica, pp. 143–151.
Del Río, L., Gracia, F.J., 2013. Error determination in the photogrammetric assessment of shoreline changes. Nat. Hazards 65, 2385–2397. https://doi.org/10.1007/s11069-012-0407-y.
Del Vecchio, S., Jucker, T., Carboni, M., Acosta, A.T.R., 2017. Linking plant communities on land and at sea: the effects of Posidonia oceanica wrack on the structure of dune vegetation. Estuar. Coast Shelf Sci. 184, 30–36. https://doi.org/10.1016/j.ecss.2016.10.041.
Del Vecchio, S., Marbà, N., Acosta, A., Vignolo, C., Traveset, A., 2013. Effects of Posidonia Oceanica beach-cast on germination, growth and nutrient uptake of coastal Dune plants. PLoS One 8. https://doi.org/10.1371/journal.pone.0070607.
Dolan, R., Fenster, M.S., Holme, S.J., 1991. Temporal analysis of shoreline recession and accretion. J. Coast Res. 7, 723–744.
Enríquez, A.R., Marcos, M., Falqués, A., Roelvink, D., 2019. Assessing beach and dune erosion and vulnerability under sea level rise: a case study in the Mediterranean Sea. Front. Mar. Sci. 6. https://doi.org/10.3389/fmars.2019.00004.
Fernández-Montblanc, T., Duo, E., Ciavola, P., 2020. Dune reconstruction and revegetation as a potential measure to decrease coastal erosion and flooding under extreme storm conditions. Ocean Coast Manag. 188. https://doi.org/10.1016/j.ocecoaman.2019.105075.
Fernandez-Mora, A., Gomez-Pujol, L., Coco, G., Orfila, A., 2025. Hydrodynamic conditions of Posidonia oceanica seagrass berm formation and dismantling events. Sci. Total Environ. 958. https://doi.org/10.1016/j.scitotenv.2024.178005.
Feyisa, G.L., Meilby, H., Fensholt, R., Proud, S.R., 2014. Automated water extraction index: a new technique for surface water mapping using landsat imagery. Remote Sens. Environ. 140, 23–35. https://doi.org/10.1016/J.RSE.2013.08.029.
Gómez-Pujol, L., Orfila, A., Álvarez-Ellacuría, A., Terrados, J., Tintoré, J., 2013. Posidonia oceanica beach-cast litter in mediterranean beaches: a coastal videomonitoring study. J. Coast Res. 165 (1), 1768–1773. https://doi.org/10.2112/si65-299.
Harley, M., 2017. Coastal storm definition. In: Ciavola, P., Coco, G. (Eds.), Coastal Storms: Processes and Impacts. Wiley, pp. 1–21. https://doi.org/10.1002/9781118937099.ch1.
Harley, M.D., Ciavola, P., 2013. Managing local coastal inundation risk using real-time forecasts and artificial dune placements. Coast. Eng. 77, 77–90. https://doi.org/10.1016/j.coastaleng.2013.02.006.
Himmelstoss, E.A., Henderson, R.E., Kratzmann, M.G., Farris, A.S., Survey, U.S.G., 2021. Digital Shoreline Analysis System (DSAS) version 5.1. Open File Rep.
Himmelstoss, E.A., Henderson, R.E.H., Kratzmann, M.G., Farris, A.S., 2018. Digital Shoreline Analysis System (DSAS) Version 5.0 User Guide. Reston, Virginia.
Hunt, E., Davidson, M., Steele, E.C.C., Amies, J.D., Scott, T., Russell, P., 2023. Shoreline modelling on timescales of days to decades. Cambridge Prisms: Coastal Futures 1. https://doi.org/10.1017/cft.2023.5.
Jiménez, M.A., Beltran, R., Traveset, A., Calleja, M.L., Delgado-Huertas, A., Marbà, N., 2017. Aeolian transport of seagrass (Posidonia oceanica) beach-cast to terrestrial systems. Estuar. Coast Shelf Sci. 196, 31–44. https://doi.org/10.1016/j.ecss.2017.06.035.
Manca, E., Pascucci, V., Deluca, M., Cossu, A., Andreucci, S., 2013. Shoreline evolution related to coastal development of a managed beach in Alghero, Sardinia, Italy. Ocean Coast Manag. 85, 65–76. https://doi.org/10.1016/j.ocecoaman.2013.09.008.
Martín Prieto, J.Á., Roig Munar, F.X., Rodríguez Perea, A., Pons Buades, G.X., Mir Gual, M., Gelabert Ferrer, B., 2018. Análisis de la evolución histórica de la línea de costa de la playa de es Trenc (S. de Mallorca): causas y consecuencias. GeoFocus Revista Internacional de Ciencia y Tecnología de la Información Geográfica 187–214. https://doi.org/10.21138/GF.544.
Martzikos, N.T., Prinos, P.E., Memos, C.D., Tsoukala, V.K., 2021. Statistical analysis of Mediterranean coastal storms. Oceanologia 63, 133–148. https://doi.org/10.1016/J.OCEANO.2020.11.001.
Menicagli, V., Balestri, E., Bernardini, G., Barsotti, F., Fulignati, S., Raspolli Galletti, A. M., Lardicci, C., 2024. Beach-cast seagrass wrack: a natural marine resource improving the establishment of dune plant communities under a changing climate. Mar. Pollut. Bull. 201. https://doi.org/10.1016/j.marpolbul.2024.116270.
Moore, L.J., 2000. Shoreline mapping techniques. Source. J. Coast Res. 16, 111–124.
Palomar-Vázquez, J., Pardo-Pascual, J.E., Almonacid-Caballer, J., Cabezas-Rabadán, C., 2023. Shoreline analysis and extraction tool (SAET): a new tool for the automatic extraction of satellite-derived shorelines with subpixel accuracy. Remote Sens (Basel) 15. https://doi.org/10.3390/rs15123198.
Pardo-Pascual, J.E., Almonacid-Caballer, J., Ruiz, L.A., Palomar-Vázquez, J., 2012. Automatic extraction of shorelines from Landsat TM and ETM+ multi-temporal images with subpixel precision. Remote Sens. Environ. 123, 1–11. https://doi.org/10.1016/j.rse.2012.02.024.
Quang, D.N., Ngan, V.H., Tam, H.S., Viet, N.T., Tinh, N.X., Tanaka, H., 2021. Long-term shoreline evolution using dsas technique: a case study of Quang Nam province, Vietnam. J. Mar. Sci. Eng. 9. https://doi.org/10.3390/jmse9101124.
Ranasinghe, R., 2016. Assessing climate change impacts on open sandy coasts: a review. Earth Sci. Rev. https://doi.org/10.1016/j.earscirev.2016.07.011.
Ranasinghe, R., Turner, I.L., 2006. Shoreline response to submerged structures: a review. Coast. Eng. 53, 65–79. https://doi.org/10.1016/J.COASTALENG.2005.08.003.
Regione Autonoma della Sardegna, 2025. Sardinia geoportale website [WWW Document]. URL. www.sardegnageoportale.it, 2.17.25.
Rizzo, A., De Giosa, F., Donadio, C., Scardino, G., Scicchitano, G., Terracciano, S., Mastronuzzi, G., 2022. Morpho-bathymetric acoustic surveys as a tool for mapping traces of anthropogenic activities on the seafloor: the case study of the Taranto area, southern Italy. Mar. Pollut. Bull. 185, 114314. https://doi.org/10.1016/J.MARPOLBUL.2022.114314.
Roig-Munar, F.X., Prieto, J.Á.M., Pintó, J., Rodríguez-Perea, A., Gelabert, B., 2019. Coastal management in the Balearic Islands. In: Morales, J. (Ed.), The Spanish Coastal Systems. Springer, Cham. https://doi.org/10.1007/978-3-319-93169-2_33.
Romine, B.M., Fletcher, C.H., 2013. A summary of historical shoreline changes on Beaches of Kauai, Oahu, and Maui, Hawaii. J. Coast Res. 29, 605–614. https://doi.org/10.2112/JCOASTRES-D-11-00202.1.
Ruggiero, P., Kaminsky, G., 2003. Linking proxy-based and Datum-Based shorelines on a high-energy coastline: implications for shoreline change analyses. J. Coastal Res. Special Issue (38), 57–82.
Sabato, G., Scardino, G., Kushabaha, A., Chirivi, M., Luparelli, A., Scicchitano, G., 2023. Deep learning-based segmentation techniques for coastal monitoring and seagrass banquette detection. In: 2023 IEEE International Workshop on Metrology for the Sea; Learning to Measure Sea Health Parameters, MetroSea 2023 - Proceedings. Institute of Electrical and Electronics Engineers Inc., pp. 524–527. https://doi.org/10.1109/MetroSea58055.2023.10317577
Sánchez-González, J.F., Sánchez-Rojas, V., Memos, C.D., 2011. Wave attenuation due to Posidonia oceanica meadows. J. Hydraul. Res. 49, 503–514. https://doi.org/10.1080/00221686.2011.552464.
Sierra, J.P., Gracia, V., Astudillo, C., Cáceres, I., Mösso, C., Sánchez-Arcilla, A., 2025. Assessment of coastal protection provided by seagrass beach cast deposits: laboratory experiments. Coastal Eng. Proc. 20. https://doi.org/10.9753/icce.v38.papers.20.
Simeone, S., 2008. Posidonia oceanica banquettes removal: sedimentological, geomorphological and ecological implications. Ph.D. Thesis, Università Degli Studi Della Tuscia. Viterbo, Italy.
Simeone, S., De Falco, G., 2013. Posidonia oceanica banquette removal: sedimentological, geomorphological and ecological implications. J. Coast Res. 1045–1050. https://doi.org/10.2112/SI65-177.
Simeone, S., Brambilla, W., Conforti, A., Meyer, F., Molinaroli, E., De Falco, G., 2024. Beach shoreline trends along the Western Coast of Sardinia Island (Western Mediterranean Sea). J. Coast Res. 113 (1). https://doi.org/10.2112/JCR-SI113-050.
Simeone, S., De Falco, G., 2012. Morphology and composition of beach-cast Posidonia oceanica litter on beaches with different exposures. Geomorphology 151–152, 224–233. https://doi.org/10.1016/j.geomorph.2012.02.005.
Simeone, S., De Muro, S., De Falco, G., 2013. Seagrass berm deposition on a Mediterranean embayed beach. Estuar. Coast Shelf Sci. 135, 171–181. https://doi.org/10.1016/j.ecss.2013.10.007.
Società Cooperativa ECO.RI.SA. (Ecologia Risanamento Sardegna), 2015. Ecorisa soc coop Arborea [WWW Document]. URL. https://www.facebook.com/ecorisa.arborea, 2.1.25.
Stefano Orrú, 2020. *Spiaggia di Arborea - Zona 32^*, 2020, September. https://maps.app.goo.gl/hEDRz4uU9PKcFmeE6.
Trogu, D., Simeone, S., Ruju, A., Porta, M., Ibba, A., DeMuro, S., 2023. A four-year video monitoring analysis of the Posidonia oceanica banquette dynamic: a case Study from an urban microtidal Mediterranean Beach (Poetto Beach, Southern Sardinia, Italy). J. Mar. Sci. Eng. 11. https://doi.org/10.3390/jmse11122376.
Vacchi, M., De Falco, G., Simeone, S., Montefalcone, M., Morri, C., Ferrari, M., Bianchi, C.N., 2017. Biogeomorphology of the Mediterranean Posidonia oceanica seagrass meadows. Earth Surf. Process. Landf. 42, 42–54. https://doi.org/10.1002/esp.3932.
Vaidya, A.M., Kori, S.K., Kudale, M.D., 2015. Shoreline response to coastal structures. Aquat Procedia 4, 333–340. https://doi.org/10.1016/J.AQPRO.2015.02.045.
Vitousek, S., Buscombe, D., Vos, K., Barnard, P.L., Ritchie, A.C., Warrick, J.A., 2023. The future of coastal monitoring through satellite remote sensing. Cambridge Prisms: Coastal Futures 1. https://doi.org/10.1017/cft.2022.4.
Vos, K., Harley, M.D., Turner, I.L., Splinter, K.D., 2023a. Pacific shoreline erosion and accretion patterns controlled by El Niño/Southern Oscillation. Nat. Geosci. 16, 140–146. https://doi.org/10.1038/s41561-022-01117-8.
Vos, K., Splinter, K.D., Harley, M.D., Simmons, J.A., Turner, I.L., 2019. CoastSat: a google Earth engine-enabled python toolkit to extract shorelines from publicly available satellite imagery. Environ. Model. Software 122. https://doi.org/10.1016/j.envsoft.2019.104528.
Vos, K., Splinter, K.D., Palomar-Vázquez, J., Pardo-Pascual, J.E., Almonacid-Caballer, J., Cabezas-Rabadán, C., Kras, E.C., Luijendijk, A.P., Calkoen, F., Almeida, L.P., Pais, D., Klein, A.H.F., Mao, Y., Harris, D., Castelle, B., Buscombe, D., Vitousek, S., 2023b. Benchmarking satellite-derived shoreline mapping algorithms. Commun. Earth Environ. 4. https://doi.org/10.1038/s43247-023-01001-2.
Xu, H., 2006. Modification of normalised difference water index (NDWI) to enhance open water features in remotely sensed imagery. Int. J. Rem. Sens. 27, 3025–3033. https://doi.org/10.1080/01431160600589179.
Yilmaz, O.S., 2023. Automatic detection of water surfaces using K-means++ clustering algorithm with Landsat-9 and Sentinel-2 images on the google Earth engine platform. Bilge Int. J. Sci. Technol. Res. 7, 105–111. https://doi.org/10.30516/bilgesci.1262550.
Zambrano-Medina, Y.G., Plata-Rocha, W., Monjardin-Armenta, S.A., Franco-Ochoa, C., 2023. Assessment and forecast of shoreline change using geo-spatial techniques in the gulf of California. Land 12. https://doi.org/10.3390/land12040782.